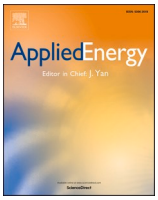
Applied Energy 382 (2025) 125261



Contents lists available at ScienceDirect

Applied Energy

journal homepage: www.elsevier.com/locate/apenergy





Assessment of dispatching scenarios for a multi-tower concentrating solar power plant in a Renewable Energy Community

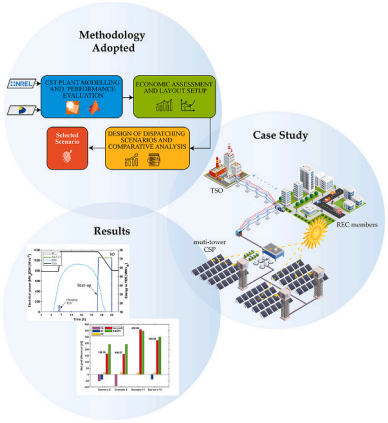
Francesco Rovense [a,b,c,*], Anna Pinnarelli [e], José González-Aguilar [c], Manuel Romero [c], Giovanni Brusco [e], Pasquale Vizza [e], Daniele Menniti [e], Nicola Sorrentino [e], Javier Dufour [b,d]

[a] ENEA, Casaccia Research Centre, Via Anguillarese 301, 00123 Rome, Italy
[b] Department of Chemical, Energy and Mechanical Technology, Rey Juan Carlos University, Calle Tulipán, 28933 Móstoles, Spain
[c] High Temperature Processes Unit, IMDEA Energy, Avda Ramón de la Sagra, 3, 28935 Móstoles, Spain
[d] Systems Analysis Unit, IMDEA Energy, Avda Ramón de la Sagra, 3, 28935 Móstoles, Spain
[e] Department of Mechanical, Energy and Management Engineering, University of Calabria, Via Pietro Bucci, 87036, Rende, Italy

HIGHLIGHTS

- An original Dispatching Scenario Selection Methodology for CSP plants was presented
- A case study of a REC integrating a multi-tower CSP plant was examined
- Best unitary configuration exhibits a Levelized Cost of Electricity of 12.42 c€/kWh
- Three single-unit CSP plants are needed to meet the REC members' demand
- Scenario providing ancillary services allows for the highest net profit of 430 k€

GRAPHICAL ABSTRACT



ARTICLE INFO

Keywords:
Concentrating solar tower
Dispatching scenario
Ancillary services, renewable energy community

ABSTRACT

Concentrating Solar Power (CSP) plants represent a promising solution for flexible and dispatchable power generation, enabling a significant increase in the share of renewable energy in electricity production. However, an effective grid-integrated CSP solution requires careful assessment of plant design and power dispatching to maximize operators' profits while adhering to local regulations. This study introduces a novel methodology for designing and selecting the operational scenarios of a CSP plant to maximize the operator's profits within a national market framework. A case study of a multi-tower CSP system integrated within a Renewable Energy Community (REC) was considered, using real energy demand data and assuming Italian electricity prices and regulations. A numerical model was implemented to assess the CSP plant's performance, and a detailed cost analysis was conducted. The Levelized Cost of Electricity (LCOE) was calculated for fifty-six plant layouts, and the configuration with the lowest LCOE was selected to determine the plant arrangement needed to meet the REC

* Corresponding author at: ENEA, Casaccia Research Centre, Via Anguillarese 301, 00123 Rome, Italy.
E-mail address: francesco.rovense@enea.it (F. Rovense).

https://doi.org/10.1016/j.apenergy.2024.125261
Received 20 May 2024; Received in revised form 19 November 2024; Accepted 28 December 2024
Available online 7 January 2025
0306-2619/© 2024 The Authors. Published by Elsevier Ltd. This is an open access article under the CC BY-NC-ND license (http://creativecommons.org/licenses/by-nc-nd/4.0/).

members' power demand of 1 MW_e. Fifteen dispatching scenarios were designed, considering tertiary regulation ancillary services, demand following, and simple energy supply. The profit for each scenario was then evaluated, and a comparative analysis was conducted. The results, following the outlined methodology, indicate that the lowest LCOE is 12.42 c€ kWh^{-1}, and that three single-unit CSP plants are required to power the REC members. The multi-tower CSP system enables the plant operator to achieve the highest annual profit of 430 k€ by exclusively providing ancillary services to the electric grid during the evening hours.

Nomenclature

AS	Ancillary Services
AP	Afternoon Product
CO_2	Carbon Dioxide
CSP	Concentrating Solar Power
CST	Concentrating Solar power Tower
DF	Demand Following
EP	Evening Product
ES	Energy Sale
HP	High Pressure
HT	High Temperature
LP	Low Pressure
LT	Low Temperature
MGT	Micro Gas Turbine
PV	Photovoltaic
REC	Renewable Energy Community
RES	Renewable Energy Sources
TES	Thermal Energy Storage
TSO	Transmission System Operator

Symbols (Units)

EPC	Engineering and Procurement Cost [€]
EPP	Energy Purchase Price [€ kWh^{-1}]
LCOE	Levelized Cost of Electricity [€ kWh^{-1}]
O&M	Operation and Maintenance Costs [€]
PP	Premium Price [€ $year^{-1}$]
ZP	Zonal Price [€ kWh^{-1}]

Physical quantity (Units)

A	Area [m^2]
$\dot{C}$	Ratio Between Minimum and Maximum Heat Capacities [−]
C	Heat Capacities [J K^{-1}]
Cp	Specific Heat [kJ kg^{-1} K^{-1}]
DNI	Direct Normal Irradiance [W m^{-2}]
E	Energy [kWh]
J	Coefficient of Compactness [m^2 m^{-3}]
L	Length [m]
$\dot{M}$	Corrected Mass Flow Rate [m s $K^{0.5}$]
M	Mass [kg]
NTU	Number of Transfer Units [−]
P	Pressure [bar]
$\dot{Q}$	Thermal Power [kW_{th}]
T	Temperature [°C]
TES	Thermal Energy Storage [MWh_{th}]
$\dot{V}$	Volumetric Flow Rate [m^3 s^{-1}]
$\dot{W}$	Electric Power [kW_e]
U	Overall Heat Transfer Coefficient [W m^{-2} K^{-1}]

Greek letters

α	Annual Insurance Rate [−]
β	Pressure Ratio [−]
γ	Specific Heat Ratio [−]
ε	Emissivity [−]
η	Efficiency [%]
θ	Effectiveness [%]
ι	Real Interest Rate [%]
λ	Plant Operating Lifetime [Years]
ξ	Conductive Heat Transfer Coefficient [W m^{-2} K^{-1}]
ρ	Density [kg m^{-3}]
σ	Stefan Boltzmann Constant [W m^{-2} K^{-4}]
τ	Thickness [m]
ω	Shaft Speed [RPM]
Ω	Corrected Speed [RPM $K^{-0.5}$]

Subscripts.

a	Ambient
act	Actual
ap	Aperture
aux	Auxiliary
c	Compressor
charge	Charging phase
cold	Cold Side
core	Material core
DP	Dense Particles
d	Design point
direct	Direct Stream
dis	Discharging phase
e	Electric
ff	Free-Flow Cross-Sectional Area
frontal	Frontal Section
gen	Generator
hot	Hot Side
HX	Heat Exchanger Stream
j-th	j-th TES Capacity
i-th	i-th Net Electric Power
in	Inlet
inv.	Inverter
is	Isentropic
loss	Losses
max	Maximum
mec	Mechanical
min	Minimum
net	Net value
nom	Nominal
opt	Optimum
out	Outlet
rec	Receiver
reg	Regenerator
scenario	Scenario
SF	Solar Field
Sol	Solar-Driven
Stream	Stream
t	Turbine
th	Thermal
tot	Total
T100	MGT Model T100
unit	Unitary Cost
w	Wetted surface

1. Introduction

Global warming continues to intensify, with rising temperatures and increasingly frequent extreme weather events highlighting the urgent need for sustainable energy solutions [1,2]. In response, policies worldwide are increasingly promoting the development and diffusion of Renewable Energy Sources (RES) to reduce greenhouse gas emissions and mitigate climate change impacts [3]. These efforts aim to transition energy systems towards cleaner, more resilient sources, aligning with global goals for environmental sustainability and energy security. Achieving these ambitious goals requires diverse RES integration into the electric grid, though this process faces complex challenges. Predominantly, the intermittent and variable nature of RES introduces a significant degree of unpredictability in power supply, necessitating advanced grid management strategies [4] and the development of new storage technologies to handle fluctuations in power production. Moreover, the non-dispatchable nature of most RES hinders their integration into the grid due to challenges in load-following and peak-demand management [5]. Concentrated solar power (CSP) systems offer numerous advantages that help increase the share of RES generation in electricity grids and improve their stability and reliability. A key advantage of CSPs lies in their inherent Thermal Energy Storage (TES) capability with the inertia characteristics from the coupled conventional thermal power plant [6]. This feature allows for the generation and dispatching of electricity even during periods with low or no Direct Normal Irradiance (DNI), effectively addressing the challenges of intermittency and variability. Furthermore, TES enables CSP plants to integrate with generation patterns from photovoltaic (PV), wind, or fossil fuels, thus facilitating the deployment of hybrid systems [7–11]. Lastly, CSP plants can also facilitate the provision of Ancillary Services (ASs), such as frequency regulation [12], while addressing other electricity grid requirements, including peak demand periods and load-following needs. Despite these significant advantages, the Levelized Cost of Electricity (LCOE) for CSPs remains higher compared to PV and wind energy, currently limiting CSP's overall competitiveness in the RES market [13]. The fluctuating energy market rules [14], policy [15], driven by variables such as energy demand [12] and regulatory frameworks [16], are other aspects influencing the increase of CSP energy production in electricity grids. Nonetheless, boosting the generation share from CSP, can bring prosperity to local communities [17], encouraging the development of a local energy market that can reduce dependence on centralized electric grids [18]. Renewable Energy Communities (RECs) have the right to autonomously organize the sharing of renewable energy within the community and to access all eligible energy markets directly or through aggregation in a non-discriminatory manner [19], offering the benefits of self-consumption as well as the provision of ASs to the energy system [20]. Micro-scale generation is emerging as an effective solution, particularly within RECs [21]. Among CSP systems suitable for micro-scale generation, those employing Concentrating Solar power Tower (CST) technology to power Micro Gas Turbines (MGT) could offer significant advantages. These systems leverage extensive knowledge from the gas turbine and CST industries, offering benefits such as rapid start-up and shutdown, low water usage, modularity, and the use of air as an economical, non-toxic working fluid [22]. They feature a simple and compact system design [23] as well as stable, secure, and efficient generation capabilities [24,25]. These distributed generation systems, typically configured as solar hybrids, facilitate reductions in both fuel consumption and CO_2 emissions [24,26–28], with LCOE values ranging from 13 to 30 c€ kWh^{-1} [22,29,30]. Moreover, solar-only CST-MGT layouts have also demonstrated potential for flexible and dispatchable energy generation [31–34]. In this framework, an important consideration is the need for private CST plant operators to optimize the plant operation and design to maximize economic profits. Regarding the design, the techno-economic analyses, based on indicators such as the LCOE, allow for the determination of the optimal plant design [35]. As for the selection of the dispatch strategy based on the planner's objectives, three methods are generally applied: optimization-based dispatch, heuristic rule-based dispatch, and predefined dispatch [6]. Dispatch by optimization involves decision variables and can be implemented as part of joint planning for the entire electric system or independently by a local planner managing start-up and shutdown operations [12,14,36–38]. This optimization has been explored for both standalone CST plants and hybrid systems combined with wind and PV sources [39–41]. Heuristic rule-based dispatch is developed using specialized knowledge of plant operations or specific system requirements [42,43]. In a predefined dispatch model, generation adheres to a specific dispatch profile based on the plant's capacity and operator-defined criteria, such as profit maximization [6]. Profit maximization for market participants focuses on optimizing the generation schedule based on historical or forecasted electricity prices, with the plant typically treated as a price taker [44]. This method considers the operational constraints on the generation

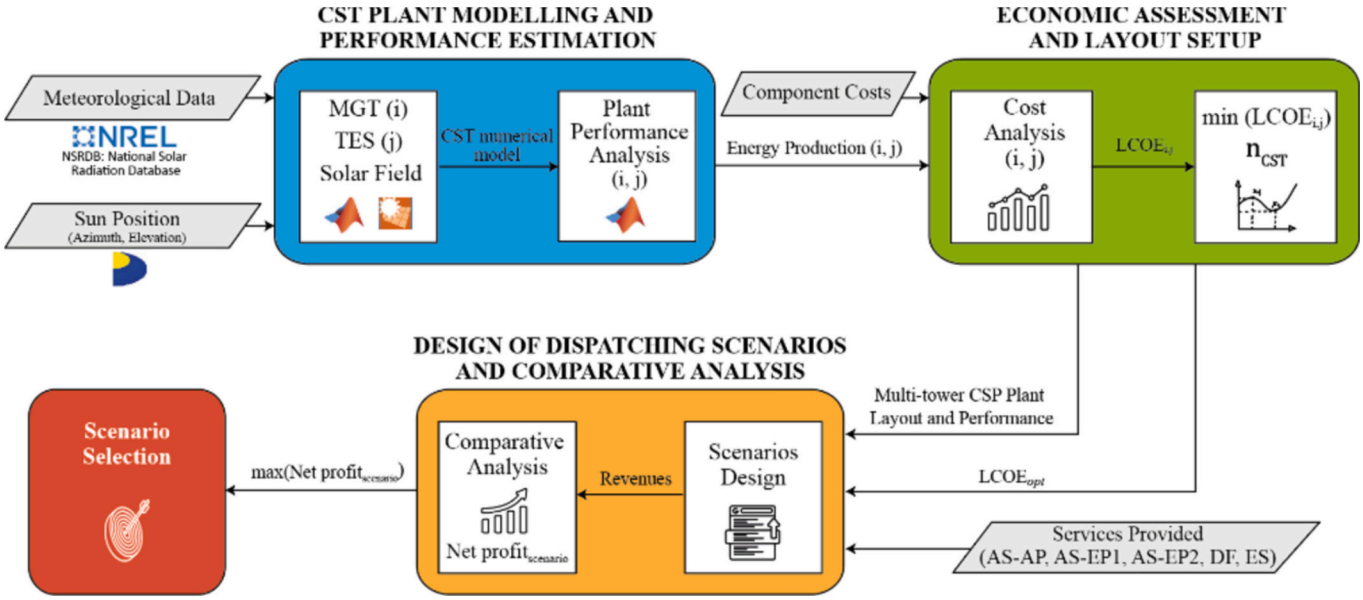


Fig. 1. Flowchart of the methodology model adopted.

side, with revenue dependent on participant roles and including profits from energy sales and ancillary services [45–47]. In this regard, a detailed analysis of the ancillary services is still lacking [46], whether they are provided independently or in combination with other grid services, such as demand following. Furthermore, the analyses conducted so far have mainly focused on generation schemes for large-scale electricity grids fed by conventional CST plants [38,48,49]. Meanwhile, a comprehensive assessment of energy systems, such as RECs, powered by micro-scale generation systems like CST-MGT, has not yet been conducted. Finally, there is a lack of a method that can encompass and integrate the aspects defined here. Therefore, the aim of this study is to present a novel methodology that enables the identification of the plant layout and the most profitable dispatching scenarios for a small-scale CST serving a REC, aiming to maximize the plant operator's profit. The main novelties introduced by this methodology include:

1) The definition of fifteen dispatching scenarios, which include tertiary regulation ancillary services, demand following, and simple energy supply;
2) A comparative analysis of scenarios, based on net profit evaluations, to identify the most economically convenient dispatching strategy for the plant operator;
3) A detailed presentation of the advantages provided by the tertiary regulation ancillary services from a CST plant and their comparative assessment against other grid services

The manuscript is structured as follows: Section 2 introduces the Theory and Calculation, encompassing the case study, Plant Modelling and Performance Estimation, Economic Assessment and Layout Setup, as well as the Design of Dispatching Scenarios and Comparative Analysis. Section 3 illustrates the main findings from the performance and economic analyses of the plant and discusses comparisons between scenarios. Finally, Section 4 presents the conclusions and outlines directions for further research.

2. Theory and calculation

Fig. 1 depicts the flowchart of the methodology model adopted in this study. *Meteorological Data* and *Sun Position*, sourced from Refs. [50,51], are the inputs to the sub-model "*CST Plant Modelling and Performance Estimation*". The numerical models of the solar receiver and the heliostat field, designed in SolarPILOT® [52] (see Appendix B), the MGT (see Appendix C), and the TES (see Appendix D), all previously validated [31,34,53,54], have been integrated into MATLAB®. This integration has allowed the development of a *CST numerical model* capable of simulating the operation of a single-unit CST plant under dynamic regime and off-design conditions. The CST plant's numerical model has enabled an analysis of the system's performance metrics, such as annual electric *Energy Production*. In the "*Economic Assessment and Layout Setup*" sub-model, *Component Costs* of the plant are the key inputs, and, taking into account the energy production of the single-unit plant, the LCOE was calculated for fifty-six different configurations, with net powers ranging from 100 to 500 kW_e and TES capacities from 5 to 35 MWh_{th}. The plant layout that achieved the *minimum LCOE,* labelled as $LCOE_{opt}$, value was selected to determine the number of single-unit CST plants needed to compose the multi-tower CSP system, in order to meet the power requirements of the REC members. Therefore, the *multi-tower CSP Plant Layout and Performance*, as well as the corresponding $LCOE_{opt}$ constitute the output of this sub-model. In the "*Design of Dispatching Scenarios and Comparative Analysis*" sub-model, the data concerning the basic *Services Provided* serve as external inputs. In this sub-model, dispatching scenarios are designed and, taking into account the unit prices of energy for each service as well as the energy produced by the multi-tower CSP plant, *Revenues* for each scenario are calculated. By considering the $LCOE_{opt}$ value as the cost of energy, net profits are determined, and a comparative analysis is conducted. The output of this sub-model is thus the *maximum Net profit*, which allows for the *Scenario Selection*. The following sections will further detail the described sub-models.

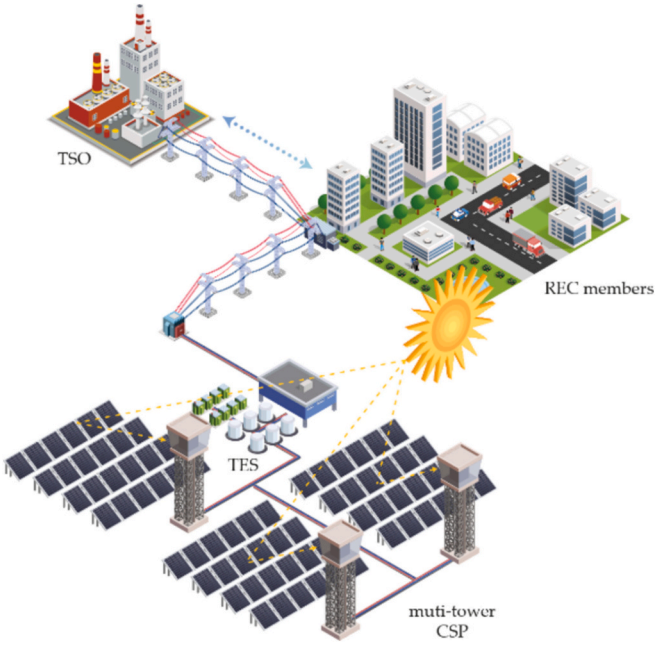


Fig. 2. Graphical representation of the considered case study.

The case study considered in this work focuses on a REC located in a city district of Cosenza, Southern Italy (39°18′N, 16°15′E), comprising residential end-users with a total peak power demand ($\dot{W}_{REC}$) of 1 MW_e. Fig. 2 provides the graphical representation of the main systems assumed. It is supposed that the REC is powered by the multi-tower CSP system, which holds dispatching priority over other power plants, including both fossil-fuelled and RES. Furthermore, the multi-tower CSP is assumed to provide various services to the electric grid, managed by the Transmission System Operator (TSO), at specific times of the day. The real electric load data, constituting the REC members' demand curve, were collected using smart meters [55].

2.1. CST plant modelling and performance estimation

The single-unit CST plant, illustrated in Appendix A, was modelled in the MATLAB® environment with one-minute step resolution, while the thermodynamic properties of air were assessed using REFPROP® [56]. It was assumed that dynamic processes in the turbomachinery occur faster than the changes in its thermodynamic boundary conditions [57]. Therefore, the overall system inertia is primarily due to the thermal inertia of components such as solar receivers and heat exchangers, and its dynamic response to changes in operational conditions does not depend on the turbomachinery. The turbomachine was assumed to be fully unfired, i.e., no combustor was employed, hence the air mass flow rate ($\dot{m}_{air}$) through both the compressor and the turbine is the same. Given a constant MGT volumetric flow rate ($\dot{V}_{MGT}$), the pressure regulation system acts to modify the air inlet compressor density ($\rho_{c,in,act}$) and, consequently, the air mass flow rate:

$$\dot{m}_{air,act} = \rho_{c,in,act}\dot{V}_{MGT} \tag{1}$$

The pressure regulation system operates to balance the actual incoming solar power ($\dot{Q}_{rec,in,act}$) and ensure a constant outlet receiver air temperature ($T_{out,rec}$):

$$\frac{\dot{m}_{air,act} - \dot{m}_{air,min}}{\dot{m}_{air,max} - \dot{m}_{air,min}} = \frac{\dot{Q}_{rec,in,act} - \dot{Q}_{rec,in,min}}{\dot{Q}_{rec,in,max} - \dot{Q}_{rec,in,min}}, \tag{2}$$

where the subscripts "act" represents the actual values of the variables, "min" and "max" denote their minimum and maximum values, respectively. Specifically for the air mass flow rate, "min" refers to ambient pressure and "max" to the maximum inlet pressure of the MGT (5.05 bar). The minimum thermal power absorbed by the receiver was set at 333 kW_{th}; this corresponds to a minimum electric power of 50 kW_e, at which the MGT can operate with an efficiency of 15 % [54]. The maximum power corresponds to the receiver's rated capacity (see Table 6 in Appendix B). The net electric power plant was calculated as follows:

$$\dot{W}_{net} = \dot{m}_{air,act}\left[\left(h_{in,t} - h_{out,t}\right)\eta_t - \left(h_{out,c} - h_{in,c}\right)\frac{1}{\eta_c}\right]\eta_{mec}\eta_{gen}\eta_{inv}, \quad (3)$$

where η_t, η_c, η_{mec}, η_{gen}, and η_{inv} are the mechanical turbine efficiency (0.95), the mechanical compressor efficiency (0.95), the mechanical efficiency (0.95), the electric efficiency (0.95), and the inverter efficiency (0.95), respectively [22]. Subscripts "t" and "c" indicate turbine and compressor, respectively, while "in" and "out" denote the inlet and outlet sections of the machines. $h_{in,c}$ is the compressor air inlet enthalpy, calculated at the compressor air inlet temperature, $T_{c,in}$ (15 °C) and at the compressor air inlet pressure, $P_{in,c}$. Similarly, $h_{out,c}$ is the compressor air outlet enthalpy, evaluated at the compressor air outlet temperature ($T_{out,c}$) and at compressor air outlet pressure ($P_{out,c}$). $h_{in,t}$ is the turbine air inlet enthalpy evaluated at the turbine air inlet temperature ($T_{in,t}$) and at the turbine air inlet pressure ($P_{in,t}$). $h_{out,t}$ is the turbine air outlet enthalpy calculated at the turbine air outlet temperature ($T_{out,t}$) and at the turbine air outlet pressure ($P_{out,t}$) (See Appendix C).

Finally, the electric efficiency was calculated as follows:

$$\eta_e = \frac{\dot{W}_{net}}{\dot{Q}_{rec,in,act}}. \quad (4)$$

Where $\dot{Q}_{rec,in,act}$ represents the actual incoming solar thermal power at the receivers' apertures, reflected by the solar field.

Solar receiver data (see Appendix B) were collected from Ref. [34] and the modules were treated as a black box with a single mass in the energy balance equation. It was assumed that the heat transfer with the air occurs inside the porous matrix of the absorbers, and that the entire air mass flow rate passes through it. Then surface absorber temperature was assumed to be the same as the air temperature leaving the absorber of the receivers ($T_{out,rec}$) [58] and it was calculated as follows:

$$M_{rec}Cp_{rec}\frac{dT_{out,rec}(t)}{dt} = \dot{Q}_{rec,in,act} - \dot{Q}_{air} - \dot{Q}_{loss}, \quad (5)$$

being M_{rec}, the mass of the receiver's absorbers, and Cp_{rec} the specific heat of the absorber material, $\dot{Q}_{rec,in,act}$ $\dot{Q}_{air}$ is the thermal power absorbed by the air, and $\dot{Q}_{loss}$ the absorbers' thermal losses.

The actual incoming solar thermal power was evaluated as follow:

$$\dot{Q}_{rec,in,act} = \eta_{SF,act}\, DNI_{act}\, A_{SF,act}, \quad (6)$$

where $\eta_{SF,act}$ is the actual heliostat field efficiency, DNI_{act} is the actual DNI, and $A_{SF,act}$ is the actual reflected area. During solar-only operation, when no air mass flow rate passes through the TES, the incident solar flux control system acts by defocusing heliostats, hence varying $A_{SF,act}$, once the threshold of 800 kW m^{-2} is exceeded. This simulation assumes a constant maintenance of solar flux and thermal power on the receiver. To regulate the net electric power produced when the TES is full and the single-unit CST system operates in solar-only mode, the heliostats' defocusing system adjusts the thermal power input to the solar receivers ($\dot{Q}_{rec,in,max}$), and subsequently the $T_{in,t}$, according to the reference MGT map presented in Ref. [54].

The thermal power absorbed by the air was calculated as follows:

$$\dot{Q}_{air} = \dot{m}_{air,act}\left(h_{in,t} - h_{out,reg,cold}\right), \quad (7)$$

where $h_{out,reg,cold}$ is the air outlet enthalpy leaving the regenerator from the cold side, calculated at the cold side regenerator air outlet temperature ($T_{out,reg,cold}$) and at the cold side regenerator air outlet pressure ($P_{out,reg,cold}$).

Given that it was assumed the presence of quartz windows sealing each aperture of the receivers (see Fig. 12 centre in Appendix B), within which the absorbers are located, their convective losses to the external ambient and to the windows were considered negligible. Following this assumption, only the radiative and conductive losses, this last occurring through the insulating material of the receivers, to the ambient were accounted. Therefore, the absorbers' thermal losses were calculated as follows:

$$\dot{Q}_{loss} = \varepsilon\, A_{ap}\, \sigma\left(T_{out,rec}^4 - T_a^4\right) + \frac{\xi}{\tau} A_{rec}\left(T_{out,rec} - T_a\right). \quad (8)$$

Here, ε is the emissivity of the absorber, A_{ap} is the total aperture area through which the solar power reflected by the heliostat field enters, (see Fig. 13 right in Appendix B), σ is the Stefan-Boltzmann constant, T_a is the ambient temperature, ξ is the conductive heat transfer coefficient of the insulation material (Rock wool), τ is the thickness of the absorber insulation, and A_{rec} is the total side area of the receivers.

To regulate $T_{in,t}$, during the charging phase of the TES, it was supposed that a portion of the air mass flow rate was directed to the TES heat exchanger stream, $\dot{m}_{air,HX}$, while the remaining mass flow was directed to the turbine ($\dot{m}_{direct\ stream}$). The by-pass ratio, which ranges between 0 and 1, was the parameter that determined these two quantities. The code calculated the by-pass ratio to achieve the required $T_{in,t}$ for generating the net electric power requested:

$$\text{by-pass ratio} = 1 - \frac{\dot{m}_{air,act} - \dot{m}_{air,HX}}{\dot{m}_{direct\ stream} - \dot{m}_{air,HX}}. \quad (9)$$

Therefore, the tool calculated $P_{in,c}$, and consequently $\dot{m}_{air,act}$, to maintain $T_{out,rec}$ constant. Thus, the energy stored in the TES was determined by these parameters. During the discharging phase of the TES, it was assumed that each MGT (in every single-unit CST plant) can ramp up linearly from zero to peak condition within fifteen minutes, as required by Italian legislation, when energy in the TES is available. Shutdown, on the other hand, was considered instantaneous.

2.2. Economic assessment and layout setup

The economic assessment was conducted to identify the system layout that allows for the lowest generation costs.

Direct costs were calculated by aggregating the costs of the main components of the single-unit CST plant:

$$Cost_{CST,i,j} = Cost_{sol-MGT} + Cost_{reg} + Cost_{gen,i} + Cost_{TES,j}, \quad (10)$$

where $Cost_{sol-MGT}$ is the cost of the solar-driven MGT, $Cost_{reg}$ is the cost of the regenerator, $Cost_{gen,i}$ is the cost of the electric generator, and $Cost_{TES,j}$ is the cost of the TES. The direct cost of the regenerator was calculated as follows:

$$Cost_{reg} = Cost_{Inconel\ 718} \cdot M_{reg}. \quad (11)$$

The costs of the electric generators were evaluated as a function of the i-th net electric power output of the single-unit CST plant [59]:

$$Cost_{gen,i} = g1 \cdot \dot{W}_{net,i}^{\ g2}. \quad (12)$$

The TES costs were evaluated for each configuration corresponding to the j-th TES capacity:

$$Cost_{TES,j} = Cost_{TES\ unit} \cdot TES_j. \quad (13)$$

A cost scaling factor (sf) was introduced to account for the solarization expenses associated with the MGT [60], and to facilitate the calculation of Operation and Maintenance (O&M) costs for the

Table 1
Assumptions of costs and items for the economic analysis.

Items	Value	Unit	Ref.
Solarized MGT Cost	192	k€	[61]
T100 MGT Cost	180	k€	[60]
Inconel 718 Cost	46	€ kg^{-1}	[62]
Constant g1	18.7	–	[59]
Constant g2	0.95	–	[59]
Heliostats Cost	88	€ m^{-2}	[63]
Tower Cost	921	€ m^{-1}	[22]
Receiver Cost	37.5	k€ m^{-2}	[64]
O&M Cost of MGT	0.015	€ kWh^{-1}	[60]
O&M Cost of CSP Plant	0.02	€ kWh^{-1}	[65]
TES Unit Cost	17.8	€ kWh^{-1}	[66]
Engineering and Procurement Costs	5%	–	[65]
Contingency Costs	10%	–	[65]
Installation Costs	15%	–	[65]
Real Interest Rate (ι)	5%	–	[67]
Plant Operating Lifetime (λ)	25	years	[67]
Annual Insurance Rate (α)	0.025	–	[67]

customized engine:

$$sf = \frac{Cost_{sol\ MGT}}{Cost_{T100\ MGT}}. \tag{14}$$

The total operation and maintenance costs for each power plant configuration were calculated by considering the O&M costs of both the modified engine and the single-unit CST plant:

$$O\&M_{CST,i,j} = (O\&M_{T100\ MGT} \cdot sf + O\&M_{CST}) \cdot E_{net,i,j}. \tag{15}$$

Here, $E_{net,i,j}$ represents the net electric energy produced by the plant for each net power configuration (i-th) and TES capacity (j-th). Installation costs were calculated as 15% of the direct single-unit CST plant costs:

$$Inst.Cost_{CST,i,j} = Cost_{CST,i,j} \cdot 0.15. \tag{16}$$

Engineering and Procurement Costs (EPC), set at 5 % of the installation costs, and contingency costs, fixed at 10% of the installation costs, were calculated as detailed below:

$$EPC_{CST,i,j} = Inst.Cost_{CST,i,j} \cdot 0.05. \tag{17}$$

$$Contingency\ Cost_{CST,i,j} = Inst.Cost_{CST,i,j} \cdot 0.1. \tag{18}$$

Finally, total plant costs were calculated as follow:

$$\begin{aligned} Tot.Cost_{CST,i,j} = & Cost_{CST,i,j} + Inst.Cost_{CST,i,j} + EPC_{CST,i,j} \\ & + Contingency\ Cost_{CST,i,j}. \end{aligned} \tag{19}$$

LCOE was then calculated for each specified single-unit CST plant power rate (i-th) and TES capacity (j-th), as follows:

$$LCOE_{i,j} = \frac{\left\{ \left[\frac{\iota \cdot (1+\iota)^{\lambda}}{(1+\iota)^{\lambda} - 1} + \alpha \right] \cdot Tot.Cost_{CST,i,j} + O\&M_{CST,i,j} \right\}}{E_{CST,i,j}}. \tag{20}$$

Table 1 enumerates the cost items assumed in the economic assessment for each component and the related references.

To determine the optimal LCOE value, the minimum calculated from the various arrangements analysed in terms of peak power and storage capacity was considered:

$$LCOE_{opt} = min\left(LCOE_{i,j}\right). \tag{21}$$

Thus, the layout corresponding to the $LCOE_{opt}$ was chosen as the optimal configuration for the single-unit CST system.

Since the peak power of a single-unit CST plant can reach a maximum of 500 kW_e, due to constraints imposed by the pressure capacity of the solar receivers and considering that this power is below $\dot{W}_{REC}$, it was necessary to determine the required number of single-unit CST plants (n_{CST}) within the multi-tower CSP system to meet the power demand. This parameter was then calculated as the ratio of the peak power demanded by the users to the power provided by a single-unit CST plant, for the configuration that allows for the achievement of the optimal LCOE, as described below:

$$n_{CST} = \frac{\dot{W}_{REC}}{\dot{W}_{net}\left(LCOE_{opt}\right)}. \tag{22}$$

The value of n_{CST} must be an integer; for this reason, the closest integer exceeding the calculated value was considered. Consequently, it was supposed that the multi-tower CSP system was composed of n_{CST} single-unit CST plants, each with the same net electric power and equipped with identical TES capacities. It is assumed that these can operate in a coordinated manner, maintaining consistent efficiency even under partial loads. Finally, it was also assumed that the systems always operate simultaneously, uniformly distributing the service to the electric grid and balancing the total load required proportionally among the various units. $LCOE_{opt}$ is not affected by n_{CST} since it is first multiplied and then divided in the LCOE calculation (see Eq. 20). Thus, it was considered that, in this particular case, the $LCOE_{opt}$ of n_{CST} power plants is equivalent to that of the single-unit CST plant.

Table 2
Main requirements for ancillary services: energy price and variable remuneration [70,71].

Ancillary service	Acronym	Time [h]	Strike Price [€ MWh_e^{-1}]	Premium Price [k€ y^{-1}]
Afternoon Product	AP	3 PM - 6 PM	200	If ≥2 h → 15.0 If ≥3 h → 22.5
Evening Product No.1	EP1	6 PM - 10 PM	400	If ≥2 h → 15.0 If ≥3 h → 22.5 If ≥4 h → 30.0
Evening Product No.2	EP2	6 PM - 10 PM	200	If ≥2 h → 15.0 If ≥3 h → 22.5 If ≥4 h → 30.0

2.3. Design of dispatching scenarios and comparative analysis

The current regulations, established by the Italian legislation, regarding the connection of power plants to the electric grid were considered. Regulating services, primarily utilized for tertiary reserve regulation, congestion management, and balancing power, require that power plants meet specific technical requirements. These include the ability to provide services within fifteen minutes of a TSO dispatch, maintain service for a minimum of two hours, and possess a minimum power plant capacity of 1 MW_e [68,69]. These services fall under the regulation of the Italian Regulatory Authority for Energy, Networks, and Environment and are categorized within a framework that delineates three types of AS, which will be referred to as "products" in the following. The regulatory framework also defines criteria such as energy pricing, the timeframe for providing services to the grid (e.g., active power), and potential additional remuneration for plant operators who offer these services [70,71].

Table 2 presents the key specifications of the ASs, including the corresponding acronyms, the time intervals during which the power plant is required to generate electricity, the energy price known as the Strike Price (SP), and the additional variable remuneration referred to as the Premium Price (PP). The first ancillary service is the Afternoon Product (AS-AP), which has a SP of 200 € MWh_e^{-1}. Power plants are required to provide this service daily from 3 PM to 6 PM. Although the plant has the flexibility to reduce the service duration to a minimum of two consecutive hours, but the balancing service provider has the authority to adjust the annual PP. Specifically, a PP of 22,500 € is awarded if the service is offered for at least three hours, and 15,000 € for at least two hours. The second ancillary service is the Evening Product No. 1

Table 3
Dispatching scenarios formulated. The word "YES" indicates the service type provided.

Scenario	AS-AP	AS-EP1	AS-EP2	DF	ES
1	YES	–	–	YES	YES
2	–	YES	–	YES	YES
3	–	–	YES	YES	YES
4	–	–	–	YES	–
5	–	–	–	YES	YES
6	–	–	–	–	YES
7	YES	–	–	–	YES
8	–	YES	–	–	YES
9	–	–	YES	–	YES
10	YES	–	–	–	–
11	–	YES	–	–	–
12	–	–	YES	–	–
13	YES	–	–	YES	–
14	–	YES	–	YES	–
15	–	–	YES	YES	–

(AS-EP1), offered by the plant daily from 6 PM to 10 PM. The plant commits to providing this service for four hours, but the balancing service provider has the authority to reduce the commitment to a minimum of two consecutive hours. In this case, the annual PP is reduced by 22,500 € for a service duration of three hours, or by 15,000 € for two hours. The SP for AS-EP1 is set at 400 € MWh_e^{-1}. The third ancillary service is the Evening Product No. 2 (AS-EP2), which is similar to AS-EP1 but with a lower SP of 200 € MWh_e^{-1}. Owing to the MGT's rapid response capability in adjusting its power output, it is assumed that the single-unit CST plant can precisely adapt its generated power to match the REC members' demand curve. This flexibility enables the provision of the Demand Following (DF) service, the price of which is based on the national Energy Purchase Price (EPP) within the Italian energy market [70]. The residual electric power, whose service provided to the grid is defined as Energy Sales (ES), is the difference between the nominal power of the multi-tower CSP system and the instantaneous power generated for the DF service. This energy is sold at the zonal price (ZP) in the area where the plant operates. The energy prices considered in this analysis are based on the Italian energy market for the year 2021 [72], which is also the year when the data were collected from the REC.

Considering the services that can be provided to the electric grid (ASs), to the REC members (DF and ES), and the constraints imposed by Italian legislation, this study formulated fifteen dispatch scenarios, as presented in Table 3. These scenarios are derived from either a combination of all or some of the basic services, such as AS-AP, AS-EP1, AS-EP2 (as detailed in Table 2), DF, and ES. This formulation, through a comparative analysis of net economic profit, enables the identification of the most advantageous dispatching strategy for the multi-tower CSP plant. It evaluates whether it is more profitable to operate under various dispatching schemes, benefiting from different energy prices and extending the plant's operational hours despite higher generation costs, or to produce electricity following a defined strategy that ensures adequate remuneration while also effectively balancing production costs.

To carry out the comparative analysis among the scenarios in order to identify the most profitable one, the net profit for each scenario was calculated using the following equation:

$$\text{Net profit}_{\text{scenario}} = \text{Price}_{\text{scenario}} \cdot E_{\text{scenario}} - \text{LCOE}_{\text{opt}} \cdot E_{\text{scenario}} + \text{PP}. \quad (23)$$

The terms $\text{Price}_{\text{scenario}}$ denotes the electricity price of the considered scenario, and E_{scenario} represents the energy produced by the multi-tower CSP plant for that scenario. To enable a homogeneous comparison, LCOE_{opt} was assumed in all cases. To better illustrate how these scenarios were formulated and the comparative analysis conducted, scenarios 1 and 11 are described as examples. Scenario 1 involves a multi-tower CSP plant offering AS-AP, DF, and ES services during specific time periods. The revenue streams in this scenario include energy sales at the SP (200 € MWh_e^{-1}) for AS-AP, at the EPP for DF, and at the ZP for ES. Additionally, revenue is generated from the PP if the plant consistently meets the required production every day of the year. Conversely, Scenario 11 exclusively involves the provision of the AS-EP1 service, with a corresponding energy selling price of 400 € MWh_e^{-1}, and includes the possibility of additional revenues from the PP.

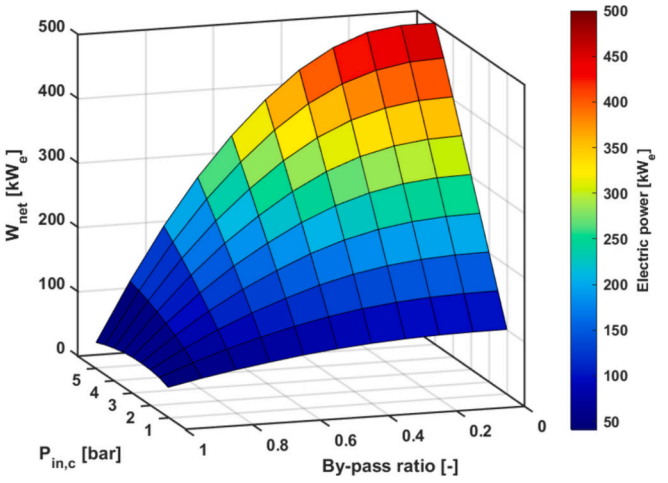


Fig. 3. Net power output trend as a function of By-pass ratio and compressor air inlet pressure.

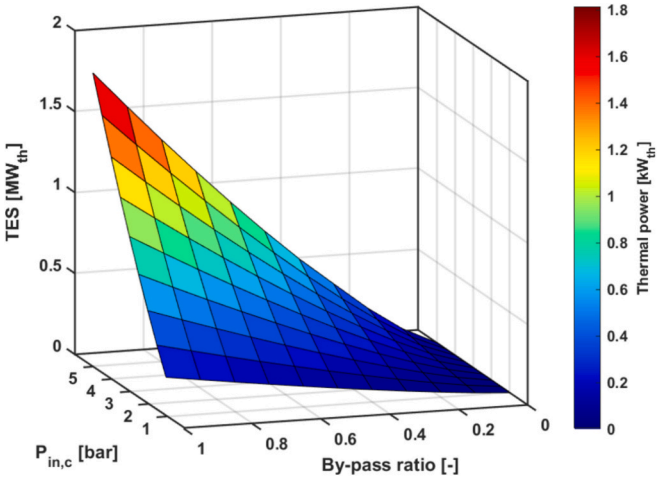


Fig. 4. Stored thermal power trend as a function of compressor air inlet pressure and By-pass ratio.

3. Results and discussion

3.1. Single-unit CST plant performance

Fig. 3 displays the net electric power trend as a function of compressor air inlet pressure and by-pass ratio for the single-unit CST plant. It was observed that an increase in compressor air inlet pressure and a reduction in the by-pass ratio led to maximized net power output. Notably, a peak power of 500 kW_e is attained at 5.05 bar when the air mass flow rate flows directly to the turbine (i.e., by-pass ratio = 0), and the TES system is not being charged.

Fig. 4 depicts the stored thermal power trend as a function of the by-pass ratio and compressor air inlet pressure. An increase in either the pressure or the by-pass ratio resulted in higher rate being stored within the TES system. Fig. 3 and Fig. 4 demonstrate the operational dynamics of the management system, revealing an inverse relationship between

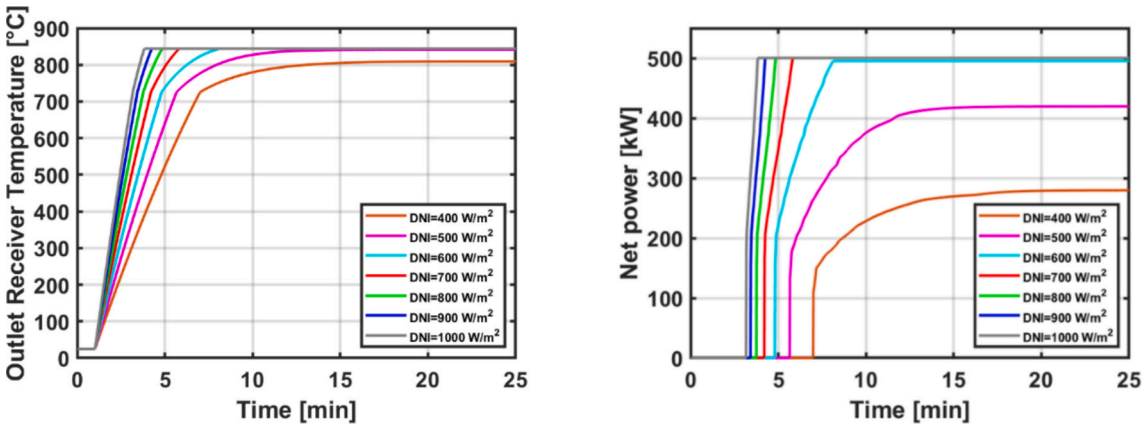


Fig. 5. (Left) Outlet receiver air temperature trend; (Right) Net power output evolution during the start-up phase versus time for different DNIs.

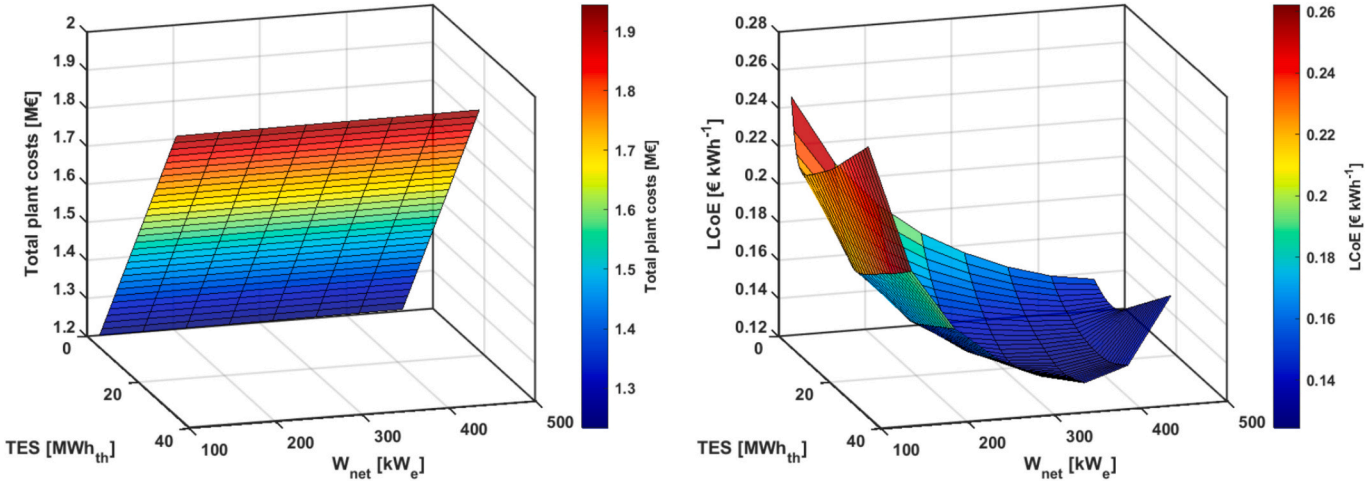


Fig. 6. (Left) Total plant costs and (Right) LCOE trends as functions of TES capacity and net power output.

net power production and that stored in the TES. This inverse relationship arose because an increase in power output led to a reduction in the rmal power directed towards TES. This was attributed to the need for the $T_{in,t}$ to be close to its nominal value, which resulted in a decreased air mass flow rate to the TES path.

Fig. 5 (left) and (right) display $T_{out,rec}$ and the $\dot{W}_{net}$ over time, respectively. These figures demonstrate the performance of a single-unit CST system during the start-up phase, assuming nominal efficiency of the solar field and bypassing the TES system. Under these conditions, air passes directly from the solar receivers to the turbine, and without transferring thermal power to the TES, the turbine inlet temperature, $T_{in,t}$, matches the $T_{out,rec}$. The analysis reveals limitations in the plant's capacity to reach peak nominal power with a DNI below 600 W m^{-2} (cyan lines). This limitation is due to the pressure regulation (not shown in these figures), which, by not reaching maximum values, restricts the maximum mass flow rate of air and thus prevents the MGT from generating nominal electric power. Conversely, a DNI above 700 W m^{-2} (red lines) allows the achievement of $T_{out,rec}$, and thus $T_{in,t}$, of 850 °C, as it facilitates the maximum mass flow rate, thereby facilitating the production of nominal power. In terms of start-up times, the plant reaches nominal power in less than ten minutes with a DNI above 700 W m^{-2} and in less than four minutes for DNIs above 800 W m^{-2}. For a threshold value of 350 kW_e, a DNI of 400 W m^{-2} is sufficient to achieve the required power. These results confirm the single-unit CST plant's capability to meet the temporal requirements set by Italian legislation, particularly regarding the tertiary regulation ancillary service.

Table 4
Economic Analysis Results and Optimal Plant Configuration.

Items	Value	Unit
$LCOE_{opt}$	12.42	c€ kWh^{-1}
Single-unit CST $\dot{W}_{net}$	350	kW_e
Single-unit CST TES	26	MWh_{th}
n_{CST}	2.85 ~ 3	–
Multi-tower CSP $\dot{W}_{net}$	1.05	MW_e
Multi-tower CSP TES capacity	78	MWh_{th}

3.2. Cost assessment results and plant layout configuration

Fig. 6 (left) and (right) illustrate the total costs of the plant and LCOE trends as functions of $\dot{W}_{net}$ and TES capacity for a single-unit CST system, respectively. An increase in both TES capacity and net power resulted in higher total plant costs. The minimum LCOE, labelled as $LCOE_{opt}$, was 12.42 c€ kWh^{-1}, which was achieved with a single-unit CST system featuring a net power of 350 kW_e and a TES capacity of 26 MWh_{th}.

Table 4 presents the optimised plant layout data. The calculated n_{CST} was 2.85; however, considering the requirement for an integer value, three power plants were necessary to feed the REC with the multi-tower CSP system. Consequently, the nominal power rate and the total TES capacity of the plant were set at 1.05 MW_e and 78 MWh_{th}, respectively.

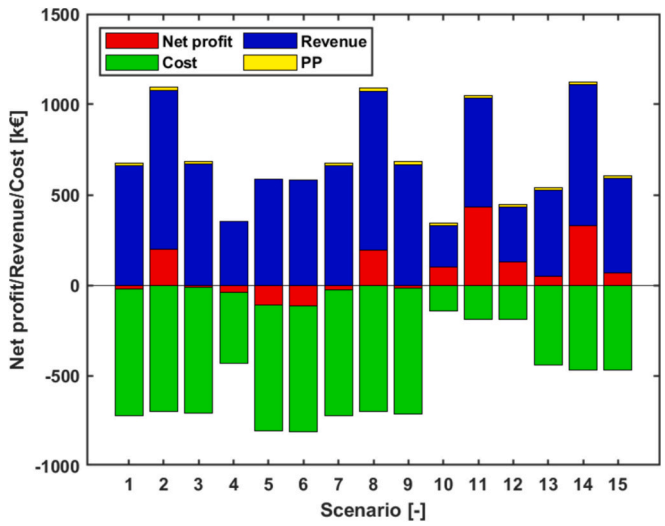


Fig. 7. Net profit, revenue, cost and premium price bars for scenarios from 1 to 15.

3.3. Dispatching scenario comparison and selection

Fig. 7 displays the net profit (represented by red bars), revenues (blue bars), costs—indicating the product of $LCOE_{opt}$ and energy produced for the considered scenario (green bars)—and PP (yellow bars, if AS were offered for at least two hours daily) for all the analysed scenarios related to the multi-tower CSP plant. In all scenarios where ASs were provided, the power plant consistently ensured a minimum of two consecutive hours of production each day, resulting in a PP of 15,000 €. Among the scenarios, those in which the plant offered AS-EP1 (scenarios 2, 8, 11, 14) consistently yielded positive net profits. This contrasts with other scenarios (1, 3, 7, 9, 10, 12, 13, 15) and scenarios that did not provide AS (4, 5, 6), which resulted in negative profits. Given that scenarios 2, 8, 11, and 14 have allowed the highest net profits, further discussions were primarily focused on these four cases.

Fig. 8-a illustrates the operating hours of the multi-tower CSP plant, while Fig. 8-b displays the net energy produced for each scenario in the four cases. In both figures, the total amount is represented by red bars, the hours/energy related to the ES service are shown with purple bars, the DF service with blue bars, and AS-EP1 with green bars.

Fig. 9 displays the net profits (red bars) and revenues from AS-EP1 (green bars), PP (yellow bars), ES (purple bars), and DF (blue bars) for the detailed cases. Scenarios 2, 8, and 14, which also provided DF and/or ES services, had the lowest net profits because the production of energy for these services did not generate profits but rather losses, since the costs of producing energy during those periods exceeded the revenues derived from the associated sale prices. Scenario 11 achieved the highest net profit (430,000 €) as the multi-tower CSP plant operated for only a few hours (1436 h; see Fig. 8-a), and incurred reduced generation costs (187,170 €; see Fig. 7). It also benefited from the highest SP of AS-EP1 (400 € MWh^{-1}) and the achievement of PP. In contrast, scenario 14, which included DF and AS-EP1, operated for a greater number of hours (3603 h) but did not yield a higher net profit than scenario 11. These results highlighted the higher profitability of supplying electricity for AS-EP1 compared to DF or ES, as the SP and PP made it more economically advantageous.

Fig. 10 (a-d) displays the key operational parameters of the multi-tower CSP system for scenarios 2, 8, 11, and 14 on July 21st. This date was selected as it is the day of the summer solstice in the Northern Hemisphere, the longest day of the year in terms of hours of solar irradiance. This means that under ideal conditions, there is maximum availability of DNI, making this day ideal for assessing the maximum production capacity of the multi-tower CSP plant. Additionally, during the summer solstice, the sun reaches its highest elevation angles in the sky, both before and after solar noon, enabling the best performance of the heliostat field. Furthermore, based on the selected meteorological

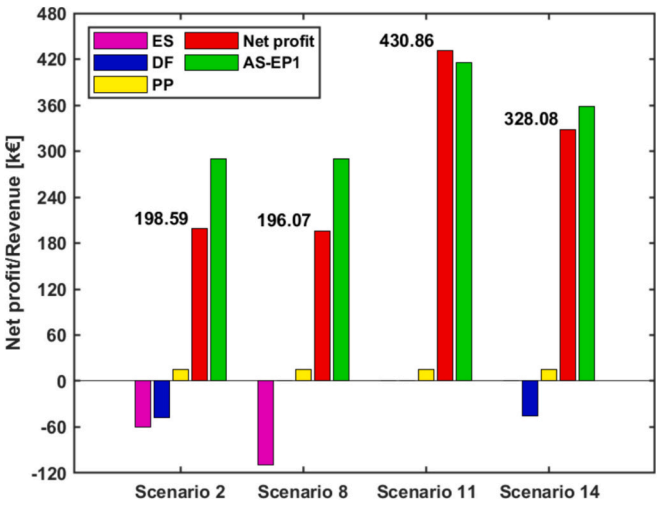


Fig. 9. Net profit and revenue for the multi-tower CSP plant for scenarios 2, 8, 11 and 14.

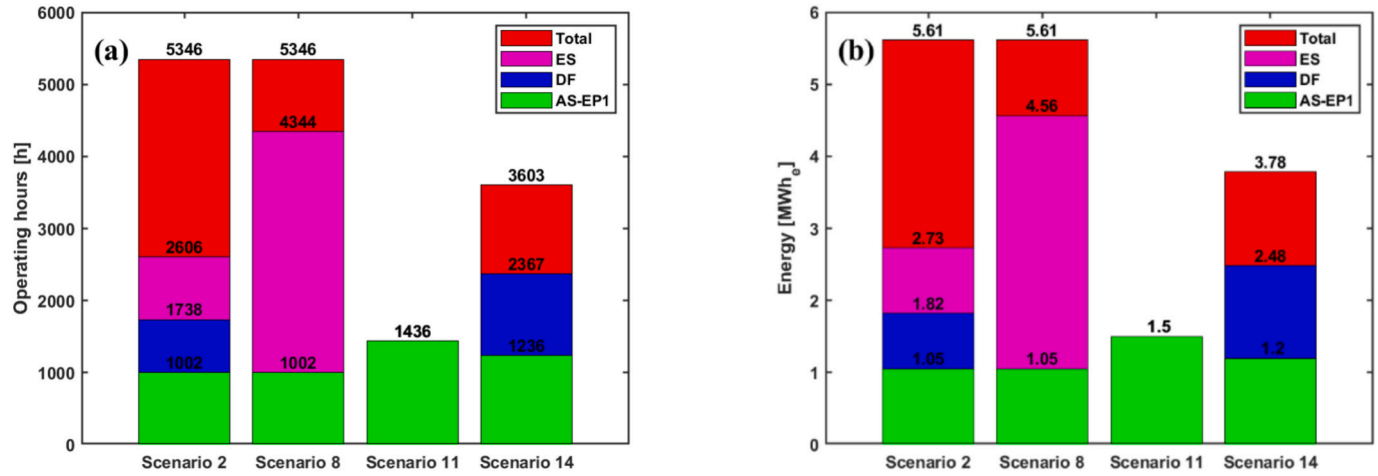


Fig. 8. Scenarios 2–8–11-14: (a) Operating hours, and (b) Energy produced.

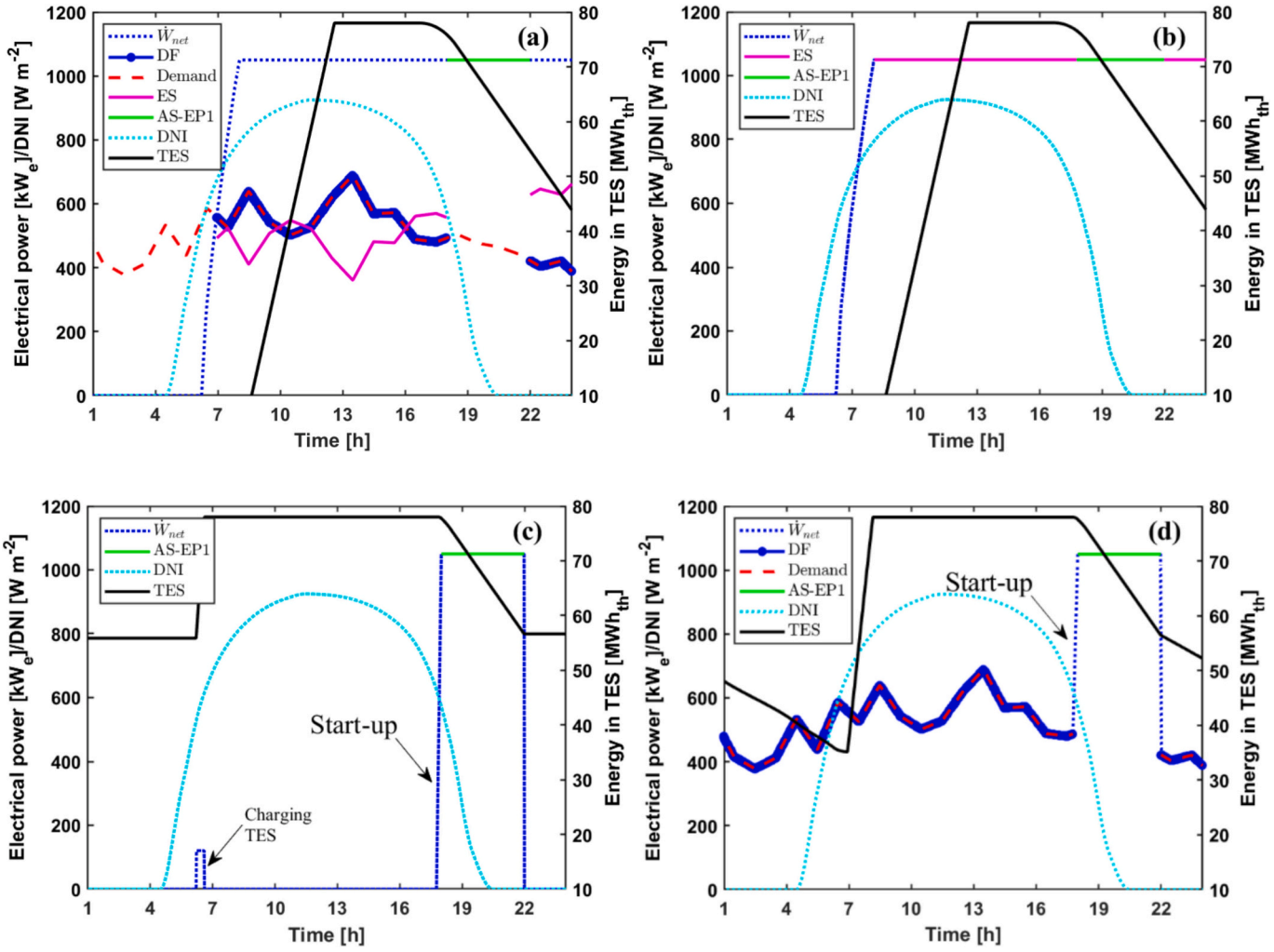


Fig. 10. Multi-tower concentrating solar power plant operation on July 21st: (a) Scenario 2; (b) Scenario 8; (c) Scenario 11; and (d) Scenario 14.

data, it also represents a typical day with clear sky and no clouds, thus facilitating the illustration and comparison of the four dispatching scenarios. The generated net power output is represented by the blue dashed line, the demand of the REC members by the red dashed line, DF by the blue solid line, ES by the purple solid line, DNI by the cyan dashed line, AS-EP1 by the green solid line (left y-axis), and the TES trend by the black solid line (referred to the right y-axis). Focusing on scenario 2 (Fig. 10-a), as an example to illustrate the plant operation, the system began production around 6 AM and started providing DF and ES services from 7 AM. By 6 PM, it commenced offering the AS-EP1 service without requiring start-up. It then ceased supplying DF and ES and began charging the TES until about 12 AM. From 5 PM onwards, it started discharging the TES due to decreasing DNI. Fig. 10-c and Fig. 10-d further illustrate the start-up operation for the AS-EP1 service, during which no other service was supplied to the grid, and the energy produced was included in the calculation of generation costs. Fig. 10-c shows the plant the plant running at minimum power (150 kW$_e$) before 7 AM exclusively to charge the TES.

4. Conclusions

This study introduced a novel methodology for assessing the design and operations, through the selection of dispatching scenarios, of a multi-tower CSP power plant integrated within a REC. The numerical model of the system was developed, and a cost assessment was conducted. The LCOE was calculated for fifty-six plant configurations; the lowest value allowed for the definition of the system layout to meet the power requirements of the REC members. Fifteen dispatching scenarios were designed as a simple combination of ancillary services, demand following, and energy sales. The net profit for each scenario was evaluated, and a comparative analysis enabled the selection of the dispatching scenario that maximizes the plant operator's profit.

The results, following the outlined methodology, indicated that the multi-tower CSP system, composed of three single-unit CST plants, which allows the lowest LCOE of 12.42 c€ kWh^{-1}, is required to meet the peak power demand of the REC members. The comparative analysis revealed that scenario 11, which exclusively offered AS-EP1, yielded the greatest net profit of 430 k€, due to the favourable Strike Price, additional revenues from the Premium Price, limited operating hours, and consequently low generation costs.

This study demonstrated that integrating a multi-tower CSP system into a REC could be a profitable strategy to increase the share of energy production from RES in electric grids. Moreover, the results indicated that providing tertiary regulation ancillary services, especially during evening hours, is the most advantageous dispatching strategy compared to other grid services. However, this study was exclusively limited to evaluating the design and operations of the multi-tower CSP system in the REC, without considering other energy sources. Therefore, further research will focus on analysing hybrid PV/Wind-CSP systems, associated with social and environmental life cycle assessments.

CRediT authorship contribution statement

Francesco Rovense: Writing – original draft, Visualization, Validation, Software, Methodology, Investigation, Funding acquisition, Formal analysis, Data curation, Conceptualization, Writing – review & editing. **Anna Pinnarelli:** Writing – review & editing, Supervision, Resources, Methodology, Investigation. **José González-Aguilar:** Writing – review & editing, Writing – original draft, Supervision, Project administration, Methodology, Investigation, Funding acquisition, Conceptualization. **Manuel Romero:** Writing – review & editing, Supervision, Software, Project administration, Funding acquisition, Formal analysis, Data curation, Conceptualization. **Giovanni Brusco:** Writing – review & editing, Writing – original draft, Visualization, Supervision, Software, Data curation, Conceptualization. **Pasquale Vizza:** Writing – original draft, Visualization, Data curation. **Daniele Menniti:** Writing – review & editing, Writing – original draft, Supervision, Methodology, Conceptualization. **Nicola Sorrentino:** Writing – review & editing, Writing – original draft, Visualization, Supervision. **Javier Dufour:** Writing – review & editing, Visualization, Supervision, Resources, Project administration, Methodology, Funding acquisition, Formal analysis, Conceptualization.

Declaration of competing interest

The authors declare that they have no known competing financial interests or personal relationships that could have appeared to influence the work reported in this paper.

Acknowledgement

This project has received funding from the European Union's Horizon 2020 research and innovation programme under the Marie Skłodowska-Curie grant agreement No 754382. The authors wish to thank "Comunidad de Madrid" and European Structural Funds for their financial support to ACES2030-CM project (S2018/EMT-4319).

Appendix A. Single-Unit CST Plant Layout description

Fig. 11 depicts the layout of the single-unit CST plant, which uses air and olivine particles as heat transfer fluid and storage medium, respectively. The solar collection system comprises a solar tower, a receiver, and a heliostats field. The MGT engine consists of a compressor, a turbine, a regenerator, an electric generator, and an inverter. The TES system is composed of a High Temperature (HT) and Low Temperature (LT) tanks, and an air-particles heat exchanger. The other main components include the pressure regulation and management systems, and the heat ejector.

Table 5 lists the technical specifications of the single-unit CST power plant under nameplate conditions, as established in previous analyses [54].

The thermodynamic cycle starts when air is compressed and flows into the regenerator (point 2), where it is preheated by the air exiting the turbine, and subsequently heated in the solar receiver. The pressure regulation system acts to maintain a constant air temperature at the receiver outlet (point 3) at about 850 °C under peak conditions [73]. In Fig. 11, the black dashed line indicates the control connection between the pressure regulation system and that point. The air is then directed to the TES (point 4), where a management system controls the fraction of the air flow rate passing through the heat exchanger using a valve. This regulation enables the control of the turbine inlet temperature, $T_{in,t}$ (point 5), thereby adjusting the power generated by the MGT to match the requirements of the electric grid. Once the air expands in the turbine, it passes through the regenerator (point 6) and enters the heat ejector (point 9) to reset the air to the compressor inlet temperature. The pressure regulation system consists of a High Pressure (HP) and a Low Pressure (LP) tank, an auxiliary compressor, and several valves. It operates by adjusting the base cycle air pressure at point 1. If the incoming thermal power to the solar receiver increases, the internal pressure rises, and air is transferred from the HP tank (point 8) to the main cycle. Conversely, air is transferred from point 7 to the LP tank.

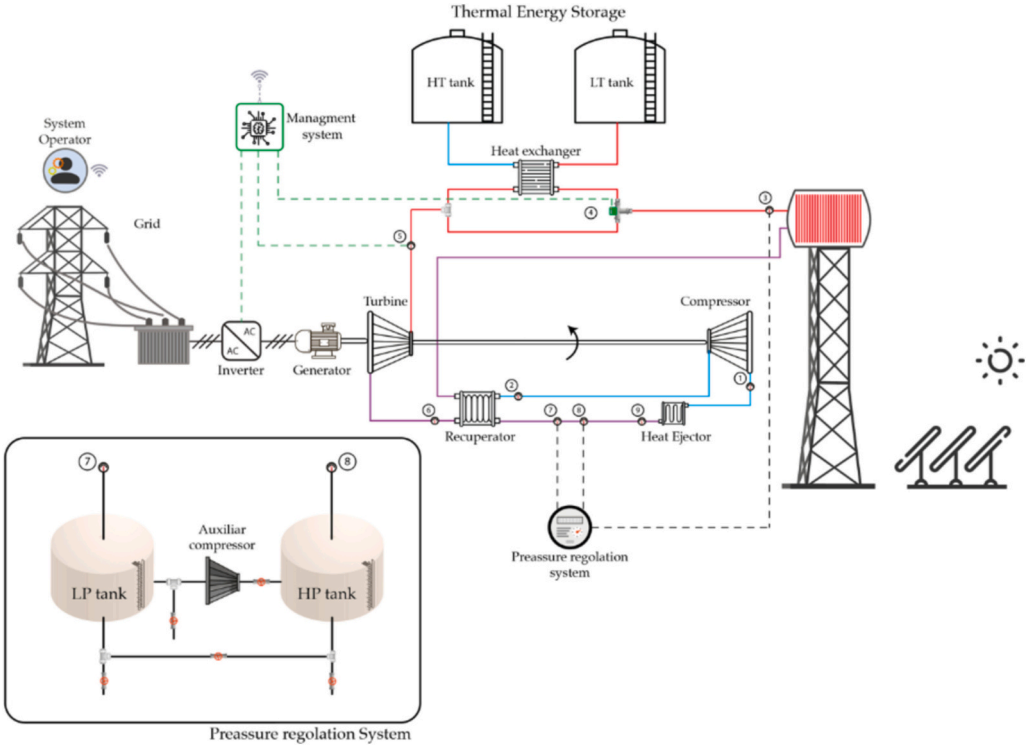


Fig. 11. Single-unit CST plant layout: main components and control systems scheme.

Table 5
Nameplate data for the single-unit CST system and its components

Parameter	Description	Value	Unit
$\dot{W}_{net,d}$	Design net electric power	500	kW_e
$\eta_{e,d}$	Design electric efficiency	0.2787	–
$\eta_{is,t,d}$	Design turbine isentropic efficiency	0.83	–
$\beta_{t,d}$	Design expansion ratio	3.27	–
$\eta_{is,c,d}$	Design compressor isentropic efficiency	0.78	–
$\beta_{c,d}$	Design Compressor isentropic efficiency	3.69	–
$T_{out,c,d}$	Design outlet compressor air temperature	181	°C
$T_{in,t,d}$	Design outlet turbine air temperature	850	°C
$\dot{M}_{t,d}$	Design corrected turbine mass flow rate	1933	$m\ s\ K^{0.5}$
$\dot{M}_{c,d}$	Design corrected compressor mass flow rate	3805.6	$m\ s\ K^{0.5}$
$\Delta P_{rec,d}$	Design pressure drops of the receiver	0.01	–
ΔP_{TES}	Design pressure drops of TES	0.07	–
$\beta_{c,aux}$	Compressor ratio of the auxiliary compressor	6.6	–
$\dot{W}_{c,aux}$	Electric power of the auxiliary compressor	153.6	kW_e
$T_{in,c,d}$	Air inlet temperature at the compressor	15	°C
$\dot{m}_{air,min}$	Minimum air mass flow rate	0.702	$kg\ s^{-1}$
$\dot{m}_{air,max}$	Minimum air mass flow rate	3.51	$kg\ s^{-1}$
$P_{rec,max}$	Maximum air pressure inside the solar receiver	30	bar

Appendix B. Solar Receiver and heliostats field design

The heliostat field was designed assuming the plant's location in Cosenza and using heliostat dimensions of 16.69 m^2 [34]. A pressurized volumetric solar receiver, consisting of four modules of a REFOS-type receiver, was considered to meet the requirements for high-pressure and high-temperature operation [58,74]. The operating pressure of the receiver limits the maximum inlet pressure of the MGT compressor. Since the maximum operating pressure of the receiver is 30 bars (see Table 5), the maximum compressor intake pressure is restricted to approximately five times the ambient pressure [33]. Fig. 12 (left) sketches the front view of the assumed solar receivers setup and their main dimensions [75]. Fig. 12 (centre) shows a section of a single module, which includes the secondary concentrator [76]. Fig. 12 (right) showcases the practical implementation of the receivers developed within the SOLGATE project [75]. The design of the solar field aimed to meet the requirements of the intended receivers and follow the aiming strategy for distributing the incident flux within the receiver aperture. Fig. 13 (left) shows the layout of the heliostat field, and Fig. 13 (right) illustrates the distribution of the solar flux on the apertures. Finally, Table 6 presents the technical data assumed and the results of the heliostat field design for the unitary CST plant.

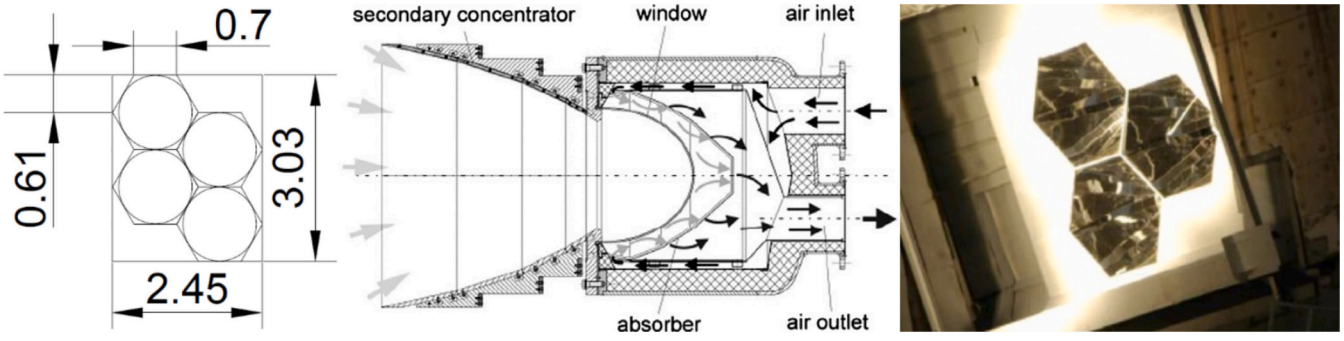


Fig. 12. (Left) Receiver aperture and front view of the four receivers and concentrators; (Centre) Solar receiver module section; (Right) Application of the solar receivers [76].

Table 6
Technical data of the heliostat field, tower, and receiver at design point.

Parameter	Value	Unit	Note
Heliostat height	5.2	m	Assumed
Heliostat width	3.21	m	Assumed
Heliostat shape	Rectangular	–	Assumed
Heliostat collision radius	3.1	m	Calculated
Number of horizontal panels	2	–	Assumed
Number of vertical panels	1	–	Assumed
Heliostat canting method	On-axis at slant	–	Assumed
Heliostat focusing type	At slant	–	Assumed
Surface slope error in X	0.0013	rad	Assumed
Surface slope error in Y	0.0013	rad	Assumed
Reflected Beam error in X	0.0002	rad	Assumed
Reflected Beam error in Y	0.0002	rad	Assumed
Total reflected image error	0.00261	rad	Calculated
Reflective surface ratio	0.92	–	Assumed
Receiver total aperture height	3.03	m	Calculated
Receiver total aperture width	2.45	m	Calculated
Receiver thermal absorbance	0.94	–	Assumed
Receiver tilt angle	19	°	Calculated
Power absorbed by air	1.794	MW_{th}	Calculated
Design DNI	890	$W\ m^{-2}$	Calculated
Peak incident flux	800	$kW_{th}\ m^{-2}$	Assumed
Design solar azimuth angle	182.57	°	Assumed
Design solar elevation angle	74.06	°	Assumed
Tower optical height	18.9	m	Calculated
Solar field nominal optical efficiency	0.675	–	Calculated
Number of heliostats	228	–	Calculated

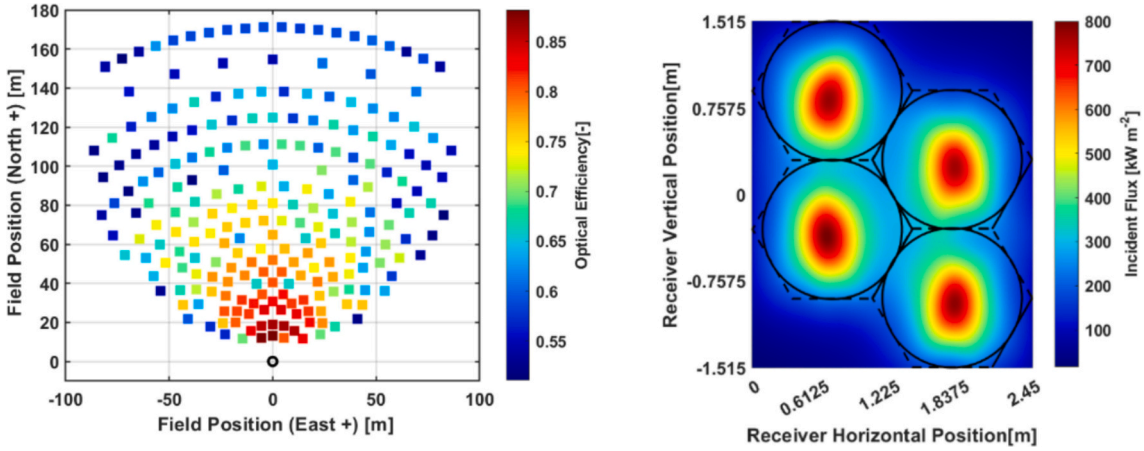


Fig. 13. (Left) Layout of the heliostat field; (Right) Receiver aperture area and aiming strategy.

Appendix C. Micro Gas Turbine Numerical Model

The compressor and turbine corrected mass flow rates ($\dot{M}_c$ and $\dot{M}_t$) and corrected speeds ($\dot{\Omega}_c$ and $\dot{\Omega}_t$) were evaluated to extrapolate the compressor ratio (β_c), turbine expansion ratio (β_t) and isentropic efficiencies ($\eta_{is,c}$ and $\eta_{is,t}$) from the static map of the MGT. This map, based on the Ansaldo Turbec T100 data [77], was implemented in an in-house tool that was validated in previous work [54].

Additionally, it was considered a single-shaft turbomachine; thus, the compressor, turbine, and electric generator operate at the same shaft speed (ω).

$$T_{out,c} = T_{in,c}\left[1+\frac{1}{\eta_{is,c}}\left(\beta_c^{\frac{\gamma-1}{\gamma}}-1\right)\right], \tag{24}$$

$$P_{out,c} = \beta_c P_{in,c}, \tag{25}$$

with γ, the air specific heat ratio. In Eqs. (24) and (25), β_c and $\eta_{is,c}$ are the pressure ratio and the isentropic efficiency of the compressor evaluated from the MGT map by calculating $\dot{M}_c$ and Ω_c:

$$\dot{M}_c = \frac{\dot{m}_{air,act}}{P_{c,in}}\sqrt{T_{c,in}}, \tag{26}$$

$$\Omega_c = \frac{\omega}{\sqrt{T_{c,in}}}. \tag{27}$$

Moreover, the turbine air outlet enthalpy, $h_{out,t}$, is evaluated at the turbine air outlet temperature ($T_{out,t}$) and at turbine air outlet pressure ($P_{out,t}$):

$$T_{out,t} = T_{in,t}\left[1 - \eta_{is,t}\left(1 - \frac{1}{\beta_t^{\frac{\gamma-1}{\gamma}}}\right)\right], \tag{28}$$

$$P_{out,t} = \frac{P_{in,t}}{\beta_t}, \tag{29}$$

where $T_{in,t}$ is the turbine air inlet temperature, $\eta_{is,t}$and $\beta_t$are the actual turbine isentropic efficiency and expansion ratio, respectively, evaluated from $\dot{M}_t$ and Ω_t:

$$\dot{M}_t = \frac{\dot{m}_{air,act}}{P_{in,t}}\sqrt{T_{out,rec}}, \tag{30}$$

$$\Omega_t = \frac{\omega}{\sqrt{T_{out,rec}}}. \tag{31}$$

$P_{in,t}$ is the turbine air inlet pressure calculated as:

$$P_{in,t} = P_{out,rec} - \Delta P_{TES}, \tag{32}$$

where ΔP_{TES} represents the overall TES system pressure drop, accounted for when air passes through the TES system, and $P_{out,rec}$ is the air receiver outlet pressure:

$$P_{out,rec} = P_{out,reg,cold} - \Delta P_{rec}, \tag{33}$$

where ΔP_{rec} is the receiver pressure drop and $P_{out,reg,cold}$ is the regenerator air outlet pressure:

$$P_{out,reg,cold} = P_{out,c} - \Delta P_{reg,cold}, \tag{34}$$

with $\Delta P_{reg,cold}$, representing the pressure drops on the cold side of the regenerator.

For the regenerator, a cross-flow heat exchanger was assumed, and reference data from Ref. [54] were considered. The actual effectiveness of the regenerator, θ, was evaluated as follows:

$$\theta = 1 - exp\left\{\frac{NTU^{0.22}}{\dot{C}}\left[exp\left(-\dot{C}\,NTU^{0.78}\right) - 1\right]\right\}, \tag{35}$$

where $\dot{C}$ is the ratio between the maximum and minimum air heat capacities, NTU is the number of transfer units:

$$NTU = \frac{UA_{tot}}{C_{min}}. \tag{36}$$

U is the overall heat transfer coefficient, $C_{min}$is the minimum of the air heat capacities and A_{tot} is the total heat transfer area:

$$A_{tot} = \frac{JL_{tot}A_{front}}{NTU}, \tag{37}$$

where J is the coefficient of compactness (i.e., the ratio of heat transfer surface to internal volume), L_{tot} is the total length of the regenerator, and A_{front} is the total frontal section, given by:

$$A_{front} = A_{ff,hot} + A_{ff,cold} + A_{core,hot} + A_{core,cold}, \tag{38}$$

where $A_{ff,hot}$ and $A_{ff,cold}$ are the free-flow crossed areas, $A_{core,hot}$ and $A_{core,cold}$ are the transversal hot and cold surfaces of the regenerator core, respectively. The off-design performance of the regenerator was emulated assuming that it is modular and that the free-flow cross-sectional area varies linearly with the air mass flow rate circulating inside [54,78]. Supposing this, the area changes as the ratio between the actual air mass flow and the maximum one:

$$\frac{\dot{m}_{air,(hot,cold),act}}{\dot{m}_{air,(hot,cold),max}} = \frac{A_{ff,(hot,cold),act}}{A_{ff,(hot,cold),d}}. \tag{39}$$

In Eq. (39) the subscripts “hot, cold” are used to respectively indicate the parameters of the regenerator sides through which the fluid flows at higher and lower temperature.

The outlet temperature of the air leaving the regenerator from the cold side ($T_{out,reg,cold}$) is then calculated as follow:

$$T_{out,reg,cold} = \theta\left(T_{out,t} - T_{out,c}\right) + T_{out,c}, \tag{40}$$

while the air outlet temperature of the hot side of the regenerator, $T_{out,reg,hot}$, is evaluated using the energy balance equation [24]:

$$M_{reg}Cp_{reg}\frac{dT_{out,reg,hot}(t)}{dt} = \tag{41}$$

$$U_{hot}A_{w,hot}\left[\frac{\left(T_{out,t} - T_{out,reg,hot}\right)}{2} - T_{M_{reg}}\right] - U_{cold}A_{w,cold}\left[T_{M_{reg}} - \frac{\left(T_{out,c} - T_{out,reg,cold}\right)}{2}\right],$$

with M_{reg}, the mass of regenerator core; Cp_{reg}, the specific heat of the regenerator core (Inconel 718) [79]; $T_{M_{reg}}$, the average temperature of the regenerator core; $U_{hot}$and U_{cold}, the overall heat transfer coefficients of hot-side and cold-side; and $A_{w,hot}$ and $A_{w,cold}$, the overall wetted areas of hot-side and cold-side.

Appendix D. Thermal Energy Storage Numerical Model

The TES was simulated using the energy balance equation between the air and the TES medium, neglecting thermal losses. Table 7 lists the data for the TES, while information regarding the validated design methodology and the main operating parameters were sourced from Refs. [31, 32, 53].

During the charging phase, when the air heats the TES media, the reference equation was:

$$M_{HX}Cp_{HX}\frac{dT_{out,HX}(t)}{dt} = \dot{m}_{air,act}\left(h_{out,rec} - h_{in,t}\right) - \dot{m}_{DP,charge}\overline{Cp}_{DP}\left(T_{in,DP,charge} - T_{out,DP,charge}\right), \quad (42)$$

while, during the discharging phase, when the TES media heats the air, the equation became:

$$M_{HX}Cp_{HX}\frac{dT_{out,HX}(t)}{dt} = \dot{m}_{DP,dis}\overline{Cp}_{DP}\left(T_{in,DP,dis} - T_{out,DP,dis}\right) - \dot{m}_{air,act}\left(h_{in,t} - h_{out,rec}\right). \quad (43)$$

In Eqs. (42) and (43), M_{HX} represents the mass of the heat exchanger core, Cp_{HX} is the specific heat of the material core, $\dot{m}_{DP}$ is the mass flow rate of the TES media, $T_{in,DP}$ is the inlet temperature, and $T_{out,DP}$ is the outlet temperature of the TES media. The subscripts "charge" and "dis" indicate the charging and discharging phases, respectively. During the charging phase, $h_{in,t}$ was regulated by the management system. In the discharging phase, $T_{in,t}$ was set according to the reference maps of MGT [54], and $P_{in,t}$ varied accordingly due to the pressure regulation system. It was assumed that the heat exchanger could ensure the temperature required for each stream [31].

Table 7
Main data for thermal energy storage system [31,32,53].

Parameter	Data	Unit
$T_{in,DP,charge,d}$	300.00	°C
$T_{out,DP,charge,d}$	820.85	°C
$T_{out,DP,dis,d}$	300.00	°C
$T_{in,DP,dis,d}$	796.85	°C
$\dot{m}_{DP,charge,d}$	2.71	kg s^{-1}
$\dot{m}_{DP,dis,d}$	2.84	kg s^{-1}
$\overline{Cp}_{DP}$	1.27	kJ kg^{-1} $°C^{-1}$

Data availability

Data will be made available on request.

References

[1] WMO. State of the Global Climate in 2022. WMO-No. 1316. 2023.
[2] Eurostat. EU economy greenhouse gas emissions: −5.3% in Q2 2023. https://ec.europa.eu/eurostat/web/products-eurostat-news/w/ddn-20231115-1; 2023.
[3] European Commission. REPowerEU. n.d.
[4] Rana MM, Uddin M, Sarkar MR, Meraj ST, Shafiullah GM, Muyeen SM, et al. Applications of energy storage systems in power grids with and without renewable energy integration — a comprehensive review. J Energy Storage 2023;68:107811. https://doi.org/10.1016/j.est.2023.107811.
[5] Meraj ST, Yu SS, Rahman MS, Hasan K, Hossain Lipu MS, Trinh H. Energy management schemes, challenges and impacts of emerging inverter technology for renewable energy integration towards grid decarbonization. J Clean Prod 2023;405:137002. https://doi.org/10.1016/J.JCLEPRO.2023.137002.
[6] Norambuena-Guzmán V, Palma-Behnke R, Hernández-Moris C, Cerda MT, Flores-Quiroz Á. Towards CSP technology modeling in power system expansion planning. Appl Energy 2024;364:123211. https://doi.org/10.1016/j.apenergy.2024.123211.
[7] Kennedy KM, Ruggles TH, Rinaldi K, Dowling JA, Duan L, Caldeira K, et al. The role of concentrated solar power with thermal energy storage in least-cost highly reliable electricity systems fully powered by variable renewable energy. Adv Appl Energy 2022;6:100091. https://doi.org/10.1016/J.ADAPEN.2022.100091.
[8] Zhang N, Yu Y, Wu J, Du E, Zhang S, Xiao J. Optimal configuration of concentrating solar power generation in power system with high share of renewable energy resources. Renew Energy 2024;220:119535. https://doi.org/10.1016/J.RENENE.2023.119535.
[9] Pilotti L, Colombari M, Castelli AFF, Binotti M, Giaconia A, Martelli E. Simultaneous design and operational optimization of hybrid CSP-PV plants. Appl Energy 2023;331:120369. https://doi.org/10.1016/j.apenergy.2022.120369.
[10] Guccione S, Guedez R. Techno-economic optimization of molten salt based CSP plants through integration of supercritical CO2 cycles and hybridization with PV and electric heaters. Energy 2023;283:128528. https://doi.org/10.1016/j.energy.2023.128528.
[11] Gutiérrez-Alvarez R, Guerra K, Haro P. Market profitability of CSP-biomass hybrid power plants: towards a firm supply of renewable energy. Appl Energy 2023;335:120754. https://doi.org/10.1016/j.apenergy.2023.120754.
[12] Abiodun K, Hood K, Cox JL, Newman AM, Zolan AJ. The value of concentrating solar power in ancillary services markets. Appl Energy 2023;334:120518. https://doi.org/10.1016/j.apenergy.2022.120518.
[13] Miron D, Navon A, Levron Y, Belikov J, Rotschild C. The cost-competitiveness of concentrated solar power with thermal energy storage in power systems with high solar penetration levels. J Energy Storage 2023;72:108464. https://doi.org/10.1016/J.EST.2023.108464.
[14] Keyif E, Hornung M, Zhu W. Optimal configurations and operations of concentrating solar power plants under new market trends. Appl Energy 2020;270:115080. https://doi.org/10.1016/j.apenergy.2020.115080.
[15] McPherson M, Mehos M, Denholm P. Leveraging concentrating solar power plant dispatchability: a review of the impacts of global market structures and policy. Energy Policy 2020;139:111335. https://doi.org/10.1016/j.enpol.2020.111335.
[16] Mena R, Escobar R, Lorca Á, Negrete-Pincetic M, Olivares D. The impact of concentrated solar power in electric power systems: A Chilean case study ☆. 2018. https://doi.org/10.1016/j.apenergy.2018.10.088.
[17] Yousef BAA, Obaideen K, AlMallahi MN, Alajmi N, Radwan A, Al-Shihabi S, et al. On the contribution of concentrated solar power (CSP) to the sustainable development goals (SDGs): a bibliometric analysis. Energ Strat Rev 2024;52:101356. https://doi.org/10.1016/J.ESR.2024.101356.
[18] Advances in renewable energy for sustainable development. 2023. https://doi.org/10.1016/j.renene.2023.119377.
[19] European Commission. Directive (EU) 2018/2001 of the European Parliament and of the council of 11 December 2018 on the promotion of the use of energy from renewable sources (recast). 2018.
[20] Brusco G, Menniti D, Pinnarelli A, Sorrentino N. Renewable energy community with distributed storage optimization to provide energy sharing and additional ancillary services. Sustain Energy, Grids Networks 2023;36:101173. https://doi.org/10.1016/j.segan.2023.101173.
[21] Tomin N, Shakirov V, Kozlov A, Sidorov D, Kurbatsky V, Rehtanz C, et al. Design and optimal energy management of community microgrids with flexible renewable energy sources *. 2021. https://doi.org/10.1016/j.renene.2021.11.024.
[22] Giostri A, Binotti M, Sterpos C, Lozza G. Small scale solar tower coupled with micro gas turbine. Renew Energy 2020;147:570–83. https://doi.org/10.1016/j.renene.2019.09.013.

[23] Olumayegun O, Wang M, Kelsall G. Closed-cycle gas turbine for power generation: a state-of-the-art review. Fuel 2016;180:694–717. https://doi.org/10.1016/j.fuel.2016.04.074.

[24] Yang J, Xiao G, Ghavami M, Al-Zaili J, Yang T, Sayma A, et al. Thermodynamic modelling and real-time control strategies of solar micro gas turbine system with thermochemical energy storage. J Clean Prod 2021;304:127010. https://doi.org/10.1016/j.jclepro.2021.127010.

[25] Chen J, Xiao G, Xu H, Zhou X, Yang J, Ni M, et al. Experiment and dynamic simulation of a solar tower collector system for power generation. Renew Energy 2022;196:946–58. https://doi.org/10.1016/j.renene.2022.07.045.

[26] Alshahrani S, Engeda A. Performance analysis of a solar-biogas hybrid micro gas turbine for power generation. J Sol Energy Eng Trans ASME 2021:143. https://doi.org/10.1115/1.4048157/1086329.

[27] Ssebabi B, Dinter F, van der Spuy J, Schatz M. Predicting the performance of a micro gas turbine under solar-hybrid operation. Energy 2019;177:121–35. https://doi.org/10.1016/J.ENERGY.2019.04.064.

[28] Nelson J, Johnson NG, Doron P, Stechel EB. Thermodynamic modeling of solarized microturbine for combined heat and power applications. Appl Energy 2018;212:592–606. https://doi.org/10.1016/j.apenergy.2017.12.015.

[29] Landman WA, Gauché P, Dinter F, Myburgh JT. Techno-economic sensitivity study of heliostat field parameters for micro-gas turbine CSP. AIP Conf Proc 2017:1850. https://doi.org/10.1063/1.4984374.

[30] Aichmayer L, Spelling J, Laumert B, Fransson T. Micro gas-turbine design for small-scale hybrid solar power plants. J Eng Gas Turbines Power 2013;135:1–11. https://doi.org/10.1115/1.4025077.

[31] Rovense F, Reyes-Belmonte MAA, González-Aguilar J, Amelio M, Bova S, Romero M. Flexible electricity dispatch for CSP plant using un-fired closed air Brayton cycle with particles based thermal energy storage system. Energy 2019;173:971–84. https://doi.org/10.1016/j.energy.2019.02.135.

[32] Rovense F, Reyes-Belmonte MA, González-Aguilar J, Amelio M, Bova S, Romero M. Application of un-fired closed Brayton cycle with mass flow regulation and particles-based thermal energy storage systems for CSP. AIP Conf Proc 2019;2126. https://doi.org/10.1063/1.5117559.

[33] Rovense F, Amelio M, Scornaienchi NMM, Ferraro V. Performance analysis of a solar-only gas micro turbine, with mass flow control. Energy Procedia, vol. 126, Elsevier B.V.; 2017, p. 675–82. doi:https://doi.org/10.1016/j.egypro.2017.08.296.

[34] Amelio M, Pèrez MS, Ferraro V, Rovense F, Bova S. Dynamic simulation of the turbine inlet temperature control system for an unfired micro gas turbine in a concentrating solar tower. Energy Procedia 2018;148:712–9. https://doi.org/10.1016/j.egypro.2018.08.161.

[35] Abdera S, Bounahmidi T, El F. Determination of design parameters to minimize LCOE, for a 1 MWe CSP plant in different sites. 2021. p. 169. https://doi.org/10.1016/j.renene.2021.01.060.

[36] Zurita A, Mata-Torres C, Cardemil JM, Guédez R, Escobar RA. Multi-objective optimal design of solar power plants with storage systems according to dispatch strategy. Energy 2021:237. https://doi.org/10.1016/j.energy.2021.121627.

[37] Kahvecioğlu G, Morton DP, Wagner MJ. Dispatch optimization of a concentrating solar power system under uncertain solar irradiance and energy prices. Appl Energy 2022;326:119978. https://doi.org/10.1016/j.apenergy.2022.119978.

[38] Wagner MJ, Hamilton WT, Newman A, Dent J, Diep C, Braun R. Optimizing dispatch for a concentrated solar power tower. Sol Energy 2018;174:1198–211. https://doi.org/10.1016/j.solener.2018.06.093.

[39] Domínguez R, Conejo AJ, Carrión M. Operation of a fully renewable electric energy system with CSP plants. Appl Energy 2014;119:417–30. https://doi.org/10.1016/j.apenergy.2014.01.014.

[40] Zhao Y, Liu S, Lin Z, Wen F, Ding Y. Coordinated scheduling strategy for an integrated system with concentrating solar power plants and solar prosumers considering thermal interactions and demand flexibilities. Appl Energy 2021;304:117646. https://doi.org/10.1016/J.APENERGY.2021.117646.

[41] Hamilton WT, Husted MA, Newman AM, Braun RJ, Wagner MJ. Dispatch optimization of concentrating solar power with utility-scale photovoltaics. Optim Eng 2020;21:335–69. https://doi.org/10.1007/s11081-019-09449-y.

[42] do Burghi ACA, Hirsch T, Pitz-Paal R. CSP dispatch optimization considering forecast uncertainties. AIP Conf Proc 2018;2033:210004. https://doi.org/10.1063/1.5067206.

[43] Wagner MJ, Newman AM, Hamilton WT, Braun RJ. Optimized dispatch in a first-principles concentrating solar power production model. Appl Energy 2017;203:959–71. https://doi.org/10.1016/j.apenergy.2017.06.072.

[44] Martinek J, Jorgenson J, Mehos M, Denholm P. A comparison of price-taker and production cost models for determining system value, revenue, and scheduling of concentrating solar power plants. Appl Energy 2018;231:854–65. https://doi.org/10.1016/j.apenergy.2018.09.136.

[45] Wittmann M, Eck M, Pitz-Paal R, Müller-Steinhagen H. Methodology for optimized operation strategies of solar thermal power plants with integrated heat storage. Sol Energy 2011;85:653–9. https://doi.org/10.1016/J.SOLENER.2010.11.024.

[46] Wang Y, Luo S, Yao L, Du E, Guan Z, Xiao X. Modeling concentrating solar power plants in power system optimal planning and operation: a comprehensive review. Sustain Energy Technol Assess 2024;71:103992. https://doi.org/10.1016/J.SETA.2024.103992.

[47] Usaola J. Participation of CSP plants in the reserve markets: a new challenge for regulators. Energy Policy 2012;49:562–71. https://doi.org/10.1016/J.ENPOL.2012.06.060.

[48] Hu B, Cai F, Tai N, Wang P. Dual-time scale optimal dispatch of the CSP-PV hybrid power plant considering dynamic operation. Energy 2024;306:132488. https://doi.org/10.1016/J.ENERGY.2024.132488.

[49] Mohammadzadeh N, Truong-Ba H, Picotti G, Cholette ME. Assessment of storage sizing for solar tower plants using model-predictive control for dispatch planning. J Sol Energy Eng Trans ASME 2024:146. https://doi.org/10.1115/1.4064504/1194222.

[50] www.sunearthtools.com. n.d. https://www.sunearthtools.com/dp/tools/pos_sun.php?lang=it#top. accessed January 10, 2022

[51] https://nsrdb.nrel.gov/data-viewer - NREL. National Solar Radiation Database. NREL 2021 [accessed October 10, 2021].

[52] Wagner MJ, Wendelin T. SolarPILOT: a power tower solar field layout and characterization tool. Sol Energy 2018;171:185–96. https://doi.org/10.1016/j.solener.2018.06.063.

[53] Reyes-Belmonte MA, Díaz E, Romero M, González-Aguilar J. Particles-based thermal energy storage systems for concentrated solar power. 2018.

[54] Rovense F, Sebastián A, Abbas R, Romero M, González-Aguilar J. Performance map analysis of a solar-driven and fully unfired closed-cycle micro gas turbine. Energy 2023;263:125778. https://doi.org/10.1016/j.energy.2022.125778.

[55] Mendicino L, Menniti D, Pinnarelli A, Sorrentino N, Vizza P, Alberti C, et al. DSO flexibility market framework for renewable energy Community of Nanogrids. Energies 2021;14:3460. https://doi.org/10.3390/en14123460.

[56] Lemmon EW, Bell Ian H, Huber ML, McLinden MO. REFPROP. 2018. https://doi.org/10.18434/T4/1502528.

[57] Caresana F, Pelagalli L, Comodi G, Renzi M. Microturbogas cogeneration systems for distributed generation: effects of ambient temperature on global performance and components' behavior. Appl Energy 2014;124:17–27. https://doi.org/10.1016/j.apenergy.2014.02.075.

[58] Buck R, Bräuning T, Denk T, Pfänder M, Schwarzbözl P, Tellez F. Solar-hybrid gas turbine-based power tower systems (REFOS). J Sol Energy Eng Trans ASME 2002;124:2–9. https://doi.org/10.1115/1.1445444.

[59] Galanti L, Massardo AF. Micro gas turbine thermodynamic and economic analysis up to 500 kWe size. Appl Energy 2011;88:4795–802. https://doi.org/10.1016/j.apenergy.2011.06.022.

[60] Montero Carrero M, De Paepe W, Parente A, Contino F. T100 mGT converted into mHAT for domestic applications: economic analysis based on hourly demand. Appl Energy 2016;164:1019–27. https://doi.org/10.1016/j.apenergy.2015.03.032.

[61] Prosin T, Pryor T, Creagh C, Amsbeck L, Uhlig R. Solar gas turbine systems with centrifugal particle receivers, for remote power generation. Energy Procedia 2015;69:1382–92. https://doi.org/10.1016/J.EGYPRO.2015.03.131.

[62] fastwell.in. Inconel 718 Price. https://www.fastwell.in/inconel-718.html; 2022.

[63] Pfahl A, Coventry J, Röger M, Wolfertstetter F, Vásquez-Arango JF, Gross F, et al. Progress in heliostat development. Sol Energy 2017;152:3–37. https://doi.org/10.1016/j.solener.2017.03.029.

[64] Schwarzbözl P, Buck R, Sugarmen C, Ring A, Marcos Crespo MJ, Altwegg P, et al. Solar gas turbine systems: design, cost and perspectives. Sol Energy 2006;80:1231–40. https://doi.org/10.1016/j.solener.2005.09.007.

[65] Spelling J, Gallo A, Romero M, González-Aguilar J. A high-efficiency solar thermal power plant using a dense particle suspension as the heat transfer fluid. Energy Procedia 2015;69:1160–70. https://doi.org/10.1016/j.egypro.2015.03.191.

[66] Rovense F, Reyes-Belmonte MÁ, Romero M, González-Aguilar J. Thermo-economic analysis of a particle-based multi-tower solar power plant using unfired combined cycle for evening peak power generation. Energy 2022;240:122798. https://doi.org/10.1016/j.energy.2021.122798.

[67] Gutiérrez RE, Haro P, Gómez-Barea A. Techno-economic and operational assessment of concentrated solar power plants with a dual supporting system. Appl Energy 2021:302. https://doi.org/10.1016/j.apenergy.2021.117600.

[68] Gulotta F, Rossi A, Bovera F, Falabretti D, Galliani A, Merlo M, et al. Opening of the Italian Ancillary Service Market to Distributed Energy Resources: Preliminary Results of UVAM project; Opening of the Italian Ancillary Service Market to Distributed Energy Resources: Preliminary Results of UVAM project. In: 2020 IEEE 17th Int Conf smart communities Improv Qual life using ICT, IoT AI; 2020. https://doi.org/10.1109/HONET50430.2020.9322822.

[69] Rancilio G, Rossi A, Falabretti D, Galliani A, Merlo M. Ancillary services markets in europe: evolution and regulatory trade-offs. Renew Sustain Energy Rev 2022;154:111850. https://doi.org/10.1016/j.rser.2021.111850.

[70] Crespi E, Colbertaldo P, Guandalini G, Campanari S. Energy storage with power-to-power systems relying on photovoltaic and hydrogen: modelling the operation with secondary reserve provision. J Energy Storage 2022;55:105613. https://doi.org/10.1016/J.EST.2022.105613.

[71] www.arera.it. Approval of the amendments, prepared by Terna S.p.A., to the pilot project for the participation of mixed virtual units in the dispatching service market (MSD), pursuant to the Authority's resolution 300/2017/R/eel - D. February 23, 2021 70/2021/R/eel. 20 2021:1–15. 2024 https://www.arera.it/allegati/docs/21/070-21.pdf (accessed September 10, 2022).

[72] Gestore dei Mercati Energetici (GME). Historical data. WWW.MERCATOELETTRICO.ORG; 2021. accessed September 12, 2022.

[73] Giovannelli A, Bashir MA. High-temperature cavity receiver integrated with a short-term storage system for solar MGTs: heat transfer enhancement. Energy Procedia 2017;126:557–64. https://doi.org/10.1016/j.egypro.2017.08.286.

[74] Požívil P, Aga V, Zagorskiy A, Steinfeld A. A pressurized air receiver for solar-driven gas turbines. Energy Procedia -SolarPACES 2013;49:498–503. https://doi.org/10.1016/j.egypro.2014.03.053. Elsevier B.V.; 2014.

[75] Directorate-General for Research and Innovation (European Commission). Solar hybrid gas turbine electric power system. 2005.

[76] Ávila-Marín AL. Volumetric receivers in solar thermal power plants with central receiver system technology: a review. Sol Energy 2011;85:891–910. https://doi.org/10.1016/j.solener.2011.02.002.

[77] Renzi M, Patuzzi F, Baratieri M. Syngas feed of micro gas turbines with steam injection: effects on performance, combustion and pollutants formation. Appl Energy 2017;206:697–707. https://doi.org/10.1016/j.apenergy.2017.08.214.
[78] Lagerström G, Xie M. High performance & cost effective recuperator for micro-gas turbines. Am Soc Mech Eng Int Gas Turbine Inst, Turbo Expo IGTI 2002;1:1003–8. https://doi.org/10.1115/gt2002-30402.
[79] Xiao G, Yang T, Liu H, Ni D, Ferrari ML, Li M, et al. Recuperators for micro gas turbines: a review. Appl Energy 2017;197:83–99. https://doi.org/10.1016/j.apenergy.2017.03.095.